

The Texas Medical Center Library
DigitalCommons@TMC

MD Anderson Cancer Center Postdoctoral
Association Annual Postdoctoral Science
Symposium Abstracts


MD Anderson Cancer Center Postdoctoral
Association

Fall 9-12-2019

9th Annual Postdoctoral Science Symposium

University of Texas MD Anderson Cancer Center PostDoctoral Association

Follow this and additional works at: https://digitalcommons.library.tmc.edu/mda_postdoc_symabs

 Part of the [Biochemistry, Biophysics, and Structural Biology Commons](#), [Cancer Biology Commons](#), [Chemistry Commons](#), [Computer Sciences Commons](#), [Development Studies Commons](#), [Genetics and Genomics Commons](#), [Immunology and Infectious Disease Commons](#), [Mathematics Commons](#), [Medicine and Health Sciences Commons](#), [Microbiology Commons](#), [Physics Commons](#), [Science and Technology Studies Commons](#), and the [Statistics and Probability Commons](#)

Recommended Citation

Citation Information: University of Texas MD Anderson Cancer Center PostDoctoral Association, "9th Annual Postdoctoral Science Symposium" (2019).

DigitalCommons@TMC, MD Anderson Cancer Center Postdoctoral Association, *MD Anderson Cancer Center Postdoctoral Association Annual Postdoctoral Science Symposium Abstracts*. Paper 2.

https://digitalcommons.library.tmc.edu/mda_postdoc_symabs/2

This Article is brought to you for free and open access by the MD Anderson Cancer Center Postdoctoral Association at DigitalCommons@TMC. It has been accepted for inclusion in MD Anderson Cancer Center Postdoctoral Association Annual Postdoctoral Science Symposium Abstracts by an authorized administrator of DigitalCommons@TMC. For more information, please contact nha.huynh@library.tmc.edu.



**PUBLICATION OF
ABSTRACTS**

**9th Annual
Postdoctoral
Science
Symposium**

Thursday, September 12 | Onstead Auditorium

Organized by the 2019 APSS Subcommittee of the MD Anderson
Postdoctoral Association

Sponsored by The Office of Postdoctoral Affairs and Development, a
unit in the Division of Education & Training

THE UNIVERSITY OF TEXAS
**MD Anderson
Cancer Center**
Making Cancer History®

Mission of the Annual Postdoctoral Science Symposium

To provide a platform for talented postdoctoral fellows throughout the Texas Medical Center to present their work to a wider audience, the MD Anderson Postdoctoral Association convened the inaugural Annual Postdoctoral Science Symposium (APSS) on August 4, 2011.

The APSS provides a professional venue for postdoctoral scientists to develop, clarify, and refine their research as a result of formal reviews and critiques by faculty and other postdoctoral scientists. Additionally, attendees discuss current research on a broad range of subjects while promoting academic interactions and enrichment and developing new collaborations.

Acknowledgements

The MD Anderson Postdoctoral Association Executive Committee (PDAEC) extends sincere gratitude to Dr. Peter WT Pisters, MD Anderson President, for his support and encouragement of all MD Anderson trainees and Dr. Stephen Hahn, Chief Medical Executive, for his continued presence and support of this annual event.

Furthermore, we thank Dr. Diane Bodurka, Chief Education and Training Officer, and the Division of Education & Training for their sponsorship of this event. We appreciate the effort required to secure the funding necessary to help establish and execute this symposium. The PDAEC also thanks the MD Anderson Postdoctoral Advisory Committee for their insights, advocacy, and mentorship throughout the year.

We recognize the contributions of Dr. Victoria McDonnell of the Office of Postdoctoral Affairs and Development, Kameshia Hunt of Graduate Medical Education, and Jenny McGee for creating professional symposium materials.

As indicated by the survey respondents, the presentations of our keynote speaker, Dr. Doris Taylor, and our invited speakers, Dr. George Calin and Dr. Philip Horner, were well-received and enlightening. We thank you all for sharing your science and time.

We are indebted to the faculty judges for their constructive evaluation of and feedback to our participants. We also thank the postdoctoral fellow judges for their feedback and review of poster and oral presentations.

Finally, a big thank you to all of the members of the PDAEC, especially our organizing committee and outgoing PDAEC chair Dr. Simone Punt, whose support helped make this event possible.

Sincerely,

A handwritten signature in cursive script that reads "Lisa Maria Mustachio".

Lisa Maria Mustachio, PhD
FY19 Chair
APSS Subcommittee
MD Anderson Postdoctoral Executive Committee

2019 APSS Organizing Committee

Lisa Maria Mustachio, PhD, Chair

Shivanand Pudakalakatti, PhD, Vice Chair

Victoria McDonnell, DrPH, ex-officio member

Members

Rajan Chaudhari, PhD

Anca Chelariu-Raicu, MD

Cynthia Kassab, MD

Vrutant Shah, PhD

Kylee Veazey, PhD

Omkara Veeranki, DVM, PhD

Competition Winners

Of the nearly 80 abstracts submitted, 12 of the submitting postdoctoral fellows were selected for oral presentations in applied science, basic science, and clinical/translational research.

Oral Competition – First-Place Winners



Applied Science: *“Mining Big Data to Estimate the Frailty Index in Patients with Congestive Heart Failure: Clinical Expert vs Machine Learning”*

[Javad Raziouyan, PhD](#)

Mentor: [Aanand Dinkar Naik, MD](#)

Project PI: [Molly Horstman, MD](#)



Basic Science: *“AXL inhibitor TP-0903 is effective against triple-negative inflammatory breast cancer and targets both tumor cells and tumor-associated macrophages”*

[Yating Cheng, PhD](#)

Mentor: [Naoto Ueno, MD, PhD](#)



Clinical/Translational Research: *“Sphingosine-kinase-1 pathway offers positive therapeutic targets in triple-negative breast cancer for effective inhibition of metastasis”*

[Sunil Acharya, PhD](#)

Mentor: [Dihua Yu, MD, PhD](#)

Poster Competition Winners

1st [Kylee Veazey, PhD](#)

A Novel Epigenetic Vulnerability in

Mentor: [Margarida Almeida Santos, PhD](#)

Non-Hodgkin B Cell Lymphoma

2nd **Daric Wible, PhD**

Somatic ATG5 mutations inactivate

Mentor: [Shawn Bratton, PhD](#)

autophagy in advanced prostate cancers by

altering a conjugation switch that controls

ATG12–ATG5-ATG16L1 complex formation

3rd **Emily Schlee Villodre, PhD**

NDRG1-EGFR axis in inflammatory breast

Mentor: [Bisrat Debeb, DVM, PhD](#)

cancer tumorigenesis and brain metastasis

Table of Contents

MISSION OF THE ANNUAL POSTDOCTORAL SCIENCE SYMPOSIUM	II
ACKNOWLEDGMENTS	III
COMPETITION WINNERS	VI
TABLE OF CONTENTS	VIII
ORAL PRESENTATIONS	1
APPLIED SCIENCE	
Poor Oral Hygiene Is Associated with HPV-Negative not HPV-Positive Oral cancer	2
3D Breast Treatment Planning Simulation: A Novel, CT-Free Approach for Low- and Middle-income Countries	5
Mining Big Data to Estimate the Frailty Index in Patients with Congestive Heart Failure: Clinical Expert vs. Machine Learning	7
BASIC RESEARCH	9
Generation of Bona Fide Prions by Large-Scale Protein Misfolding Cyclic Amplification	
Spatial Nucleus Barcoding Integrates Cellular Genomics and Tissue Architecture in Normal and Malignant Breast Tissues	11
CLINICAL/TRANSLATIONAL RESEARCH	13
Radiographic and Serologic Predictors of Pathologic Major Response to Preoperative Therapy for Pancreatic Cancer	
Sphingosine Kinase 1 Pathway Offers Positive Therapeutic Targets in Triple-Negative Breast Cancer for Effective Inhibition of Metastasis	15
POSTER PRESENTATIONS	17

A Genomic Atlas of Systemic Interindividual Epigenetic Variation in Humans	18
An Infant Mouse Intranasal Colonization Model Indicates Hyaluronic Acid Capsule Influences Streptococcus pyogenes Transmissibility and Persistence in a Serotype-Dependent Manner	20
A Novel Model to Study Metaplastic Breast Cancer	22
Bilingualism in Toddlers Born Preterm: Cognitive, Language, and Brain Development	24
Caspase-2 Regulates a Cell Cycle Checkpoint to Limit Growth of Cancer Cells	26
Decorin-Mediated Suppression of Tumorigenesis and Skin Invasion in Inflammatory Breast Cancer via Inhibition of the E-cadherin/EGFR Axis	28
Directed Neuronal Differentiation in GBM by Suppression of TAZ	31
When Will the Cancer Start? Elucidating the Correlations Between Cancer Initiation Times and Lifetime Cancer Risks	33
ENBPI Ligand for Ga-68: Synthesis, Radiolabeling Optimization, and Pilot Myocardial Perfusion Imaging with ECG-Gated PET	34
Heme Activates the Inflammatory Caspases to both Positively and Negatively Regulate Inflammation	36
Utilizing Protein Chaperone Interactions to Identify Disease Associated Mutations that Perturb Protein Folding in Cells	38
Inhibition of IRE1/XBP1 Pathway Sensitizes Triple-Negative Breast Cancer Cells to Replication Stress and Radiotherapy	40
Loss of Excitatory Cerebellar Neurons Alters Circuit Function and Causes Severe Motor Dysfunction in Neonatal Mice	42
LRP1 Is a Novel Receptor that Regulates T-Cell Proliferation	44
Monitoring Membrane Protein Trafficking in Live Cells at Endogenous Expression Levels Using a Novel Structural Complementation Assay	46
Oral Administration of Leucine Ameliorates Lipopolysaccharide-Induced Depression-Like Behavior	47

PRINCESS: Framework for Comprehensive Detection and Phasing of SNPs and SVs	49
Putting the Brakes on Translation – A Computational Study to Understand the Mechanism of Translation Inhibition by Pateamine A and Analogs	51
Mutation Status of RAS, TP53, and SMAD4 Is Superior to Mutation Status of RAS Alone for Predicting Prognosis after Resection of Colorectal Liver Metastases	53
Role of CX3CR1 Signaling in Malignant Transformation of Gliomas	55
Secondary Particle Interactions in a Compton Camera Designed for In Vivo Range Verification of Proton Therapy	57
Somatic ATG5 Mutations Inactivate Autophagy in Advanced Prostate Cancers by Altering a Conjugation Switch that Controls ATG12–ATG5-ATG16L1 Complex Formation	59
The G-Quadruplex DNA Stabilizing Drug Pyridostatin Promotes DNA Damage and Downregulates Transcription of Brca1 in Neurons	61
The Hook Complex-Associated Protein BOH1 in <i>Trypanosoma brucei</i> Cooperates with Polo-Like Kinase to Regulate Flagellum Inheritance and Cytokinesis Initiation	62
Analyzing Left-Truncated and Right-Censored HIV Cohort Data with Interval-Censored HIV Infection Onset	64
Bayesian Variable Selection in Regression with Compositional Covariates	65
Enabling Communication Between Microbe-Microelectronic Interface with Incorporated Protein Switches	66
Novel Derivatives of Anaplastic Lymphoma Kinase Inhibitors: Synthesis, Radiolabeling, and Preliminary Biological Studies of Fluoroethyl Analogues of Crizotinib, Alectinib, and Ceritinib	68
Activity of the Novel Aurora Kinase B Inhibitor AZD2811 in Biomarker-Defined Models of Small Cell Lung Cancer	70
Activity of Venetoclax-Based Therapy in TP53-Mutated Acute Myeloid Leukemia	72
Are We Appropriately Depicting Diversity: Portrayal of Skin Tone in Gender-Affirming Literature	75
Assessment of Intratumoral Heterogeneity in Early-Stage Estrogen Receptor-Positive Breast Cancer	78

Roles of Glutamate Receptors in the Retinal Calcium Influx at Connexin 36 Gap Junctions	81
IL-6 Gene Expression in Primary Acral Lentiginous Melanoma As a Clinical Prognostic Factor	83
The Gender-Nonconforming Population in a Medicaid Managed Program	85
The Pleiotropy Associated with De Novo Variants in CHD4, CNOT3, and SETD5 Extends to Moyamoya Angiopathy	87
The Relationship Between Alcohol, Physical Activity, and Obesity in Mexican-Origin Adults	90
Analyzing Astrocyte Regulation of the Blood-Brain Barrier	93
*Novel Derivatives of Anaplastic Lymphoma Kinase Inhibitors: Synthesis, Radiolabeling and Preliminary Biological Studies of Fluoroethyl Analogues of Crizotinib, Alectinib and Ceritinib	95

*Included with permission from the *European Journal of Medicinal Chemistry*.

Oral Presentations

Oral presentations were in the following categories: Applied Science, Basic Research, and Clinical/Translational Research. Each category included up to four presenters, all of whom were required to be first authors of their submitted abstracts.

Please note only abstracts of presenters who agreed to have their abstracts published are included.

APPLIED SCIENCE

Poor Oral Hygiene Is Associated with HPV-Negative not HPV-Positive Oral Cancer

Jitesh Shewale, PhD¹, Robert Pickard², Maura Gillison, MD, PhD¹

¹Department of Thoracic/Head and Neck Medical Oncology, The University of Texas MD Anderson Cancer Center, Houston, TX; ²The Ohio State University Comprehensive Cancer Center, Columbus, OH

Background: Oral health behaviors have been implicated as risk factors for oral squamous cell carcinoma (OSCC; i.e., oral cavity and oropharyngeal cancers), and we recently reported that these risk factors also dramatically alter the oral microbiome. As described herein, we performed a detailed analysis of associations between oral health behaviors and OSCC in a matched case-control study. We stratified our analysis to compare and contrast associations with human papillomavirus (HPV)-positive and -negative OSCC.

Methods: Cases were patients with newly diagnosed OSCC at The Ohio State University Comprehensive Cancer Center from 2011 to 2014. Controls were patients without cancer at the same outpatient clinic who were individually matched (2:1) with each case according to sex, age (5-year intervals), and race (white, black, or other). Cases were stratified by tumor high-risk HPV status (HPV-positive, n = 117; HPV-negative, n = 114) based on E6 or E7 mRNA expression. Data on demographics, tobacco and alcohol use, sexual history, and oral health behaviors were collected using an audio computer-assisted self-interview. Conditional logistic regression was used to

calculate odds ratios (ORs) and 95% confidence intervals (CIs), and oral health behaviors significant in univariable analysis ($p < 0.25$) were evaluated using separate multivariable models.

Results: In univariable analysis, oral health behaviors such as frequency of dental clinic visits, tooth brushing, dental flossing, and gum bleeding; tooth loss; and denture use markedly increased the risk of HPV-negative OSCC, whereas none of these behaviors increased the risk of HPV-positive OSCC. Also, in univariable analysis, covariates that independently increased the risk of HPV-negative OSCC were low income level, high lifetime number of cigarette pack-years (never-smoker, >1 - <15 , ≥ 15 - <30 , ≥ 30 - <45 , and >45), and high lifetime number of alcohol drink-years (never-drinker, <25 , ≥ 25 - <100 , ≥ 100 - <200 , and ≥ 200), whereas high lifetime number of marijuana hit-years (<10 , ≥ 10 - <50 , and ≥ 50) decreased the risk of HPV-negative OSCC. The covariates that independently increased the risk of HPV-positive OSCC were low education level and high number of oral sex partners (0-2, 3-6, and ≥ 7). After adjusting for covariates in multivariable analysis, fewer than one dental clinic visit per year independently increased the risk of HPV-negative OSCC (OR, 1.98 [95% CI, 1.05-3.75]). Dental flossing less often than once per day also independently increased the risk of HPV-negative OSCC overall (OR, 2.36 [95% CI, 1.26-4.45]) and in those without dentures (OR, 1.92 [95% CI, 1.01-3.63]). In multivariable analysis, frequency of tooth brushing and gum bleeding, denture use, and tooth loss were not associated with HPV-negative OSCC.

Conclusion: Poor oral health behaviors such as infrequent dental visits and dental flossing were independently associated with HPV-negative OSCC but not HPV-positive OSCC. These findings are consistent with the hypothesis that poor oral health behaviors alter oral microbial composition to promote chronic inflammation and the development of

HPV-negative OSCC. Thus, public health efforts in promoting good oral health behaviors would have implications for primary prevention of HPV-negative OSCC.

3D Breast Treatment Planning Simulation: A Novel, CT-Free

Approach for Low- and Middle-income Countries

Yvonne Roed, PhD¹, Rex Cardan, PhD², Simona Shaitelman, MD³, Anuja Jhingran, MD³, Daniel Craft, PhD⁴, Rebecca Howell, PhD¹, Richard Popple, PhD², Laurence Court, PhD¹

¹Department of Radiation Physics, The University of Texas MD Anderson Cancer Center, Houston, TX; ²Department of Radiation Oncology, The University of Alabama at Birmingham, Birmingham, AL; ³Department of Radiation Oncology, The University of Texas MD Anderson Cancer Center, Houston, TX; ⁴Department of Radiation Oncology, Mayo Clinic, Phoenix, AZ

Objective: Many radiation therapy centers in low- and middle-income countries lack reliable access to pretreatment imaging devices such as computed tomography (CT) simulators, which are commonly used to generate patient-specific 3D radiation treatment plans. In these situations, the dose for each breast cancer patient is calculated to only a single point based solely on the separation of the breast. We aimed to develop a low-cost, CT-free approach to patient-specific 3D breast radiation treatment planning.

Methods: A process to generate simplified, synthetic CT images using three Microsoft Kinect cameras was developed. These images are combined into a surface map from which orthogonal slices are constructed and converted into simplified, synthetic CT images. The CT images only contain information about the outer body shape without any internal anatomy. Several camera positions were investigated and optimized to provide the most reliable surface map. This system was tested using both anthropomorphic breast (n = 2) and chest wall (n = 8) phantoms, including six in-house 3D-printed chest wall phantoms (based on actual patient CT images). Distances between landmarks (e.g.,

separation between the midline and midaxillary line) were measured on synthetic and real CT images of these phantoms to assess geometric accuracy. The 3D-printed phantoms were then set up on a CT simulator in a supine breast treatment position, and real CT images were acquired, followed by acquisition of synthetic CT images. To evaluate the agreement between real and synthetic CT images, both image sets were imported into a treatment planning system and registered.

Results: The most reliable surface map was achieved when all three cameras were positioned on the ipsilateral side of the phantom facing the object at an angle of 30° from vertical and stacked with the two outer cameras about 20 cm higher than the middle camera. All measured distances on the actual and synthetic CT images differed by fewer than 5 mm (average, 1.8 ± 1.3 mm [range, 0.5-4.8 mm]). Eighty percent of all measurements were within 2 mm. Both image sets were registered by manually shifting the synthetic CT images by less than 6 cm in the inferior direction (average, 4.8 ± 0.62 cm [range, 4.3-5.5 cm]) and by less than 1 cm to the left (average, 0.9 ± 0.2 cm [range, 0.7-1.0 cm]).

Conclusion: This camera system could be an inexpensive solution for CT-free 3D breast radiation treatment planning. The system can reliably reproduce phantom geometry to within a few millimeters between actual and measured phantom geometries. Correct representation of the phantom geometry and registration of real and synthetic CT images are important first steps in developing a CT-free breast radiation treatment planning system for low- and middle-income countries. Further studies of spatial agreement metrics between real and synthetic CT images are in progress, as reliable agreement is a determining factor in generating clinically acceptable breast radiation treatment plans using only synthetic CT images.

Mining Big Data to Estimate the Frailty Index in Patients with Congestive Heart Failure: Clinical Expert vs. Machine Learning

Javad Razjouyan, PhD^{1,5,7}, Aanand D. Naik, MD^{1,2,4,5,7}, Bijan Najafi, PhD⁶, Jacqueline Shahin, MS^{1,2,5}, Salim S Virani, MD^{1,3}, Molly J Horstman, MD^{1,2,5}

¹VA HSR&D, Center for Innovations in Quality, Effectiveness and Safety, Michael E. DeBakey VA Medical Center, Houston, TX; ²Section of Health Services Research, Department of Medicine, ³Section of Cardiovascular Research, ⁴Section of Geriatrics, Department of Medicine, Baylor College of Medicine, Houston, TX; ⁵VA Quality Scholars Coordinating Center, IQuEST, Michael E. DeBakey VA Medical Center, Houston, TX; ⁶Interdisciplinary Consortium on Advanced Motion Performance (iCAMP), Division of Vascular Surgery and Endovascular Therapy, Michael E. DeBakey Department of Surgery, Baylor College of Medicine, Houston, TX; ⁷Big Data Scientist Training Enhancement Program (BD-STEP), VA Office of Research and Development, Washington, DC

Introduction: Early recognition of frailty in older adults with congestive heart failure (CHF) is needed to target interventions to slow functional decline and improve patient-centered outcomes. Previous studies used laboratory values and vital signs to measure a frailty index (FI) to predict mortality. However, variable selection was based on expert opinion alone.

Hypothesis: We hypothesize that an FI for CHF patients developed by mining laboratory values and vital signs with a machine learning algorithm will better predict mortality than will an FI developed based on expert opinion.

Methods: This was a retrospective cohort study of patients with hospital admissions for CHF in the Veterans Health Administration from 2012 to 2014. Results of outpatient

laboratory tests and vital sign measurements for which more than 50% of the cohort had reported values were collected for the year prior to admission. Two physicians reviewed the laboratory test results and vital signs and used expert opinion to determine which variables may be associated with physical frailty. The laboratory tests and vital signs were also fed into a machine learning algorithm to select variables. The accumulation of deficits method was used to calculate the FI. Cox survival models were developed with the machine learning variables, expert opinion variables, and a combination of the two. The outcome of interest was mortality. The performance of the models was compared using time-dependent area under the curve with 10-fold cross-validation.

Results: The cohort consisted of 24,457 patients (age, 72 ± 11 years; 98% male) with a 70% mortality rate in 6 years. Of 53 variables (49 laboratory test results and 4 vital signs), the physicians selected 29 variables, the machine selected 23, and the physicians and machine agreed on 14. The average area under the curve was 0.561 (95% confidence interval [CI], 0.561-0.562) for the expert opinion FI, 0.605 (95% CI, 0.604-0.606) for the machine FI, and 0.607 (95% CI, 0.606-0.608) for the combination FI.

Conclusions: The FI developed using the machine learning algorithm was a better predictor of mortality than was the FI developed based on expert opinion and used fewer variables. This study showed the potential for operationalizing an FI using laboratory values and vital signs from electronic health records. In future studies, we plan to feed additional clinical variables into the machine learning algorithm to improve the accuracy of the FI model.

BASIC RESEARCH

Generation of Bona Fide Prions by Large-Scale Protein

Misfolding Cyclic Amplification

Fei Wang, PhD, Luis Concha-Marambio, PhD, Enrique Armijo, PhD, Claudio Soto, PhD

Mitchell Center for Alzheimer's Disease and Related Brain Disorders, Department of Neurology,

McGovern Medical School at The University of Texas Health Science Center at Houston,

Houston, TX

Misfolding of the normal prion protein PrP^C into the pathogenic prion protein PrP^{Sc} is the key event causing prion diseases. However, the molecular mechanism underlying this conformational conversion remains elusive, largely due to the absence of high-resolution structural information on PrP^{Sc}, impeding the development of efficacious therapeutic strategies for these currently incurable diseases. We present herein our latest results of large-scale production of bona fide prions using protein misfolding cyclic amplification (PMCA) to facilitate structural studies of PrP^{Sc}, which not only provides a platform for ultrasensitive detection of prions in biological samples but also can faithfully reproduce the key properties of prions, including infectivity, species barriers, and strain variability. In a pilot study, normal mouse brain homogenates were seeded with RML prion in large containers to produce bona fide prions using PMCA in reaction volumes ranging from 30 to 120 mL. The prion yielded in this large-scale production maintained the RML prion strain characteristics in terms of infectivity in wild-type animals, incubation time, PrP^{Sc} biochemical profile, and pathological changes. In a follow-up study, a recombinant prion generated from bacterially expressed full-length recombinant mouse prion protein seeded with the RML prion was used to seed the large-scale production of recombinant PrP^{Sc} using PMCA. This large-scale PMCA (LS-PMCA) platform is capable of producing

at least 2 mg of PK-resistant recombinant PrP^{Sc} in a 200-mL reaction in 24 hours and can scale up to 1,000 mL per round of LS-PMCA. An infectivity assessment of the recombinant PrP^{Sc} from LS-PMCA is ongoing. Availability of a procedure to produce massive amounts of PrP^{Sc} using a recombinant protein as a substrate, which maintains the typical biological and biochemical properties of bona fide prions, will facilitate structural and biochemical studies of infectious prions.

Spatial Nucleus Barcoding Integrates Cellular Genomics and Tissue Architecture in Normal and Malignant Breast Tissues

Kaile Wang, PhD¹, Min Hu, MS¹, Shanshan Bai, MS^{1,2}, Mashiya Rabbani, MS³, Hui Chen, MD, PhD⁴, Bora Lim, MD⁵, Nicholas E. Navin, PhD^{1,6,7}

¹Department of Genetics, ²Department of Genitourinary Medical Oncology, ³School of Health Professions, ⁴Department of Pathology, ⁵Department of Breast Medical Oncology, The University of Texas MD Anderson Cancer Center, Houston, TX; ⁶MD Anderson Cancer Center UTHealth Graduate School of Biomedical Sciences, Houston, TX; ⁷ Department of Bioinformatics and Computational Biology, The University of Texas MD Anderson Cancer Center, Houston, TX

The expression programs of cell types in tissues and their spatial organization are critical for understanding homeostatic functions of normal tissues and the progression of diseases such as cancer. However, current single-cell RNA-sequencing methods inherently lose all spatial information on cellular localization. To overcome this technical obstacle, we developed a spatial nucleus barcoding (SNUBAR) technology that delivers spatial barcodes into tissue regions, after which barcoded nuclei are used for high-throughput single-nucleus RNA sequencing. We validated this method in sample barcoding and intermixing experiments with cell lines, which showed high efficiency of barcode delivery and doublet identification. We applied SNUBAR to 36 spatial regions of a normal breast tissue, which identified nine major cell types and three distinct spatial regions (fatty, fibroblast, and epithelial). The fatty region was mainly composed of adipocytes that co-localized with a distinct lipo-fibroblast expression state, whereas the fibroblast region contained matrix-producing fibroblasts that co-localized with proangiogenic macrophages and vascular endothelial cells. The epithelial areas were composed of three distinct epithelial cell types that co-localized with lymphatic

endothelial cells and another fibroblast expression program. We further applied SNUBAR to 15 spatial regions of an invasive breast tumor, which identified four cell types in the microenvironment in addition to the tumor cells. Whereas most immune and stromal cells were uniformly distributed across the 15 spatial regions, the tumor cells consisted of two distinct expression programs that were spatially segregated and harbored distinct copy-number alterations. The two tumor clones exhibited differences in gene signatures associated with epithelial-to-mesenchymal transition, MYC targets, hypoxia, and the expression of several cancer genes (e.g., VEGFA, AKT1, AKT2). Additionally, we found two distinct macrophage expression states that co-localized with different tumor subclones. These data demonstrate the utility of applying SNUBAR to delineation of the spatial organization of cell types and their expression programs in normal and malignant tissues to understand how spatial localization influences gene expression programs. This new technology is expected to have numerous applications in broad fields in which the spatial organization of cell types is key to understanding biological functions and the progression of diseased states.

CLINICAL/TRANSLATIONAL RESEARCH

Radiographic and Serologic Predictors of Pathologic Major

Response to Preoperative Therapy for Pancreatic Cancer

Giampaolo Perri, MD¹, Laura Prakash, MD¹, Huamin Wang, MD², Priya Bhosale, MD³, Gauri R. Varadhachary, MD⁴, Robert Wolff, MD⁴, David Fogelman, MD⁴, Michael Overman, MD⁴, Shubham Pant, MD⁴, Milind Javle, MD⁴, Eugene Koay, MD⁵, Joseph Herman, MD⁵, Michael Kim, MD¹, Naruhiko Ikoma, MD¹, Ching-Wei Tzeng, MD¹, Jeffrey E. Lee, MD¹, Matthew H. G. Katz, MD¹

¹Department of Surgical Oncology, ²Department of Pathology, ³Department of Diagnostic Radiology, ⁴Department of Gastrointestinal Medical Oncology, ⁵Department of Radiation Oncology, The University of Texas MD Anderson Cancer Center, Houston, TX

Objective: We sought to identify potential radiologic and serologic markers of pancreatic tumor response to therapy using pathologic major response (pMR) as the objective endpoint.

Background: We previously demonstrated that a pMR to preoperative therapy, defined as detection of less than 5% viable cancer cells in a surgical sample upon histopathologic analysis, is an important prognostic factor for patients with pancreatic ductal adenocarcinoma (PDAC).

Methods: Pretreatment and posttreatment computed tomography scans of consecutive patients who received chemotherapy and/or irradiation/chemoradiation prior to pancreatectomy for PDAC from January 2010 to December 2018 were rereviewed. Treatment response as per RECIST (version 1.1), other radiographic changes in tumor

size and anatomic extent, and posttreatment CA19-9 levels were compared in patients who did and did not have a pMR upon final histopathologic analysis of their surgical samples.

Results: A total of 290 patients with localized PDAC underwent pancreatectomy from 2010 to 2018 after receiving preoperative chemotherapy (n = 36 [12%]), irradiation/chemoradiation (n = 87 [30%]), or both (n = 167 [58%]). Among them, 28 (10%) experienced pMR, including 9 (3%) who experienced pathologic complete response. Multivariable logistic regression analysis confirmed low posttreatment CA19-9 level, partial response, and reduction in tumor volume to be independently associated with pMR (p<0.01).

Conclusions: We identified serologic and radiographic indicators of pMR that can help inform the delivery of preoperative therapy to patients with PDAC.

Sphingosine Kinase 1 Pathway Offers Positive Therapeutic Targets in Triple-Negative Breast Cancer for Effective Inhibition of Metastasis

Sunil Acharya, PhD^{1,2}, Jun Yao, PhD¹, Ping Li¹, Chenyu Zhang, PhD¹, Frank J. Lowery, PhD^{1,2}, Qingling Zhang, MD¹, Hua Guo, MD³, Jingkun Qu¹, Fei Yang, MD, PhD⁴, Ignacio I. Wistuba, MD⁴, Helen Piwnica-Worms, PhD⁵, Aysegul A. Sahin, MD³, Dihua Yu MD, PhD^{1,2}

¹Department of Molecular and Cellular Oncology, The University of Texas MD Anderson Cancer Center, Houston, TX; ²Cancer Biology Program, MD Anderson Cancer Center UTHealth Graduate School of Biomedical Sciences, Houston, TX; ³Department of Pathology, ⁴Department of Translational Molecular Pathology, ⁵Department of Experimental Radiation Oncology, The University of Texas MD Anderson Cancer Center, Houston, TX

About 10-20% of breast cancers are triple-negative, specifically, they do not express estrogen receptor, progesterone receptor, or human epidermal growth factor receptor 2 (HER2). Triple-negative breast cancer (TNBC) tends to occur at a higher frequency in younger women and is particularly aggressive, with high recurrence and metastasis rates. Compared with patients having other subtypes of breast cancer, TNBC patients have a poor overall prognosis. For example, the 5-year survival rate in patients with stage IV TNBC is about 22%, mainly due to early-onset metastasis. Because TNBCs lack expression of hormone and HER2 receptors (i.e., they are negative for therapeutic targets), they do not respond to and patients therefore cannot benefit from currently available hormone and HER2-targeted therapies. In contrast with the successful development of therapies for hormone receptor-positive and/or HER2-positive breast cancers, little progress has been made in identifying molecular targets expressed in

TNBCs that are druggable. Clearly, discovery of positive druggable targets in TNBCs is needed instead of accepting its triple-negative nontargetable status. To identify positive therapeutic targets in TNBC, we performed integrative bioinformatic analysis of multiple breast cancer patient-derived gene expression data sets and focused on kinases with U.S. Food and Drug Administration-approved or in-pipeline inhibitors. We identified sphingosine kinase 1 (SPHK1) as a top candidate. SPHK1 catalyzes phosphorylation of sphingosine, an amino alcohol, to generate sphingosine-1-phosphate, a novel lipid signaling mediator with both intracellular (as a second messenger) and extracellular (as a ligand for G protein-coupled receptors) functions. SPHK1 overexpression in human TNBC cell lines promotes spontaneous metastasis to the lungs in nude mice. Moreover, genetic knockdown of SPHK1 in TNBC patient-derived xenograft cells and TNBC cell lines decreases spontaneous metastasis to the lungs in nude mice. Using an unbiased approach, we demonstrated that fascin (FSCN1) upregulation contributes to SPHK1-driven metastasis. Mechanistically, SPHK1 transcriptionally upregulates metastasis-promoting FSCN1 gene expression via nuclear factor κ B (NF κ B) activation to promote metastasis. SPHK1/NF κ B/FSCN1 signaling pathway activation is associated with distant metastasis and poor clinical outcome in TNBC patients. Targeting SPHK1 and NF κ B with clinically applicable inhibitors (safingol and bortezomib, respectively), significantly inhibited aggressive mammary tumor growth and spontaneous lung metastasis in orthotopic syngeneic TNBC mouse models. These findings highlight SPHK1 and its downstream NF κ B as promising positive targets for effective therapeutic intervention for TNBC metastasis with fast-track clinical translation potential.

Poster Presentations

A total of 62 posters were accepted for presentation during the 2019 symposium.

Please note, only abstracts of presenters who could present during APSS and agreed to have their abstracts published are included.

A Genomic Atlas of Systemic Interindividual Epigenetic

Variation in Humans

Chathura Gunasekara, PhD¹, C. Anthony Scott, PhD¹, Eleonora Laritsky¹, Maria Baker, PhD¹, Harry MacKay, PhD¹, Jack D. Duryea¹, Noah J. Kessler^{3,4}, Garrett Hellenthal, PhD², Alexis Wood, PhD¹, Kelly Hodges, MD⁵, Manisha Gandhi, MD⁵, Amy Hair, MD⁶, Matt Silver, PhD³, Sophie Moore, PhD^{3,4}, Andrew Prentice, PhD³, Yumei Li, PhD^{7,8}, Rui Chen, PhD^{7,8}, Cristian Coarfa, PhD⁹, Robert Waterland, PhD^{1,8}

¹USDA/ARS Children's Nutrition Research Center, Department of Pediatrics, Baylor College of Medicine, Houston, TX; ²UCL Genetics Institute, Department of Genetics, Evolution and Environment, University College London, London, UK; ³MRC Unit The Gambia at London School of Hygiene and Tropical Medicine, Keneba, The Gambia; ⁴Department of Women and Children's Health, King's College London, London, UK; ⁵Department of Obstetrics and Gynecology, ⁶Department of Pediatrics – Neonatology, ⁷Human Genome Sequencing Center, ⁸Department of Molecular and Human Genetics, ⁹Department of Molecular and Cellular Biology, Baylor College of Medicine, Houston, TX

Methylation of cytosines in CpG dinucleotides (DNA methylation) is an epigenetic mechanism with essential roles in mammalian development. Because DNA methylation is established during development and stably governs gene expression potential throughout life, it is a prime candidate mechanism in the Developmental Origins of Health and Disease (DOHaD). Elaborating causal pathways in DOHaD (linking early exposures, induced epigenetic changes, and consequent disease) is complicated, however, due to the inherent cell-type specificity of most epigenetic marks. We therefore set out to identify human genomic regions exhibiting non-tissue-specific variation, in other words, systemic interindividual variation (SIV), in DNA methylation. Like genetic variation, SIV is a potential determinant of phenotype and can be assessed in any DNA

sample that can be easily analyzed via biopsy. We designed an unbiased screen for human genomic regions exhibiting SIV. We performed deep whole-genome bisulfite sequencing of genomic DNA from tissues representing all three germ layers—endoderm (thyroid), mesoderm (heart), and ectoderm (brain)—from all 10 donors from the NIH Genotype-Tissue Expression project. We developed a computational algorithm to identify genomic regions at which interindividual variation in DNA methylation is consistent across the three tissues. After evaluating the characteristics of these regions using publicly available data sets, we developed a web-based application to share this resource with the research community. We identified 9,926 correlated regions of SIV (CoRSIVs). Although making up just 0.1% of the human genome, we showed that CoRSIVs are intercorrelated over long genomic distances, associated with transposable elements and subtelomeric regions, conserved across diverse human ethnic groups, sensitive to the periconceptional environment, and associated with genes implicated in various human disorders and phenotypes. We have uncovered, characterized, and charted a previously unexplored molecular level of human individuality. Our atlas of human CoRSIVs is a valuable and timely resource for population-based investigations into epigenetic mechanisms in the DOHaD.

An Infant Mouse Intranasal Colonization Model Indicates Hyaluronic Acid Capsule Influences *Streptococcus pyogenes* Transmissibility and Persistence in a Serotype-Dependent Manner

Luis Alberto Vega, PhD¹, Misu A. Sanson, MD, PhD¹, Brittany J. Shah¹, Anthony R. Flores, MD, PhD, MPH^{1,2}

¹Division of Infectious Diseases, Department of Pediatrics, McGovern Medical School at The University of Texas Health Science Center at Houston, Houston, TX; ²Center for Antimicrobial Resistance and Microbial Genomics, The University of Texas Health Science Center at Houston, Houston, TX

Streptococcus pyogenes (group A *Streptococcus* [GAS]) is a human pathogen responsible for a range of diseases. From commonplace streptococcal pharyngitis to life-threatening necrotizing fasciitis and toxic shock syndrome, GAS-related disease constitutes a significant human health problem. In addition to causing disease, GAS can asymptotically colonize the human throat. Most GAS research is devoted to the mechanisms by which GAS causes disease, but substantial gaps in knowledge exist about the factors driving GAS transmission and colonization. The hyaluronic acid capsule contributes to GAS resistance to phagocytic immune cells, but GAS strains lacking it have been linked with enhanced colonization and persistence. To investigate factors like this capsule that influence colonization and transmission of GAS across hosts, we developed an infant mouse model of GAS intranasal colonization and transmission. Following intranasal inoculation with GAS, we monitored the mice for GAS shedding, bacterial burden, and transmission of GAS to uninoculated littermates for 11 days. In this model, persistent intranasal colonization of infant mice was inoculum size-

dependent, as was the shedding of GAS from the nares that occurred during the early phase of infection. Transmission of GAS was associated with high shedding titers during the early acute phase of intranasal colonization (days 1-3). Persistent shedding of GAS from intranasally colonized infant mice also resulted in transmission of streptococci across littermates. We detected differences in the rate of transmission and persistence across various GAS serotypes tested in our model. Similarly, the different mouse strain backgrounds used for inoculation (e.g., CD-1, C57BL/6J, FVB/NJ) exhibited differences in GAS transmission and colonization rates. We next used our model to test the hypothesis that the presence of the hyaluronic acid capsule inhibits transmission and reduces persistence by hindering adherence of GAS to host epithelia. We inoculated mice with a capsule-positive (M3) or capsule-negative (M87) GAS M type. Data derived from our model are consistent with those from human and nonhuman primate studies in that the presence of the capsule enhances shedding of GAS. However, the GAS capsule influences transmission and persistence in a strain-dependent manner. Future work using this model will examine the role of the capsule and other GAS virulence factors in manipulating the host inflammatory response, which, as evidence from studies of other Gram-positive pathogens suggests, is central to the transmission of bacteria colonizing the host nasopharynx.

A Novel Model to Study Metaplastic Breast Cancer

Vrutant Shah, PhD¹, Wendy Olivares², Pilar O'Neal³, Patrick Krause⁴, Sabrina Stratton¹,
Michelle Barton, PhD^{1,5}

¹Department of Epigenetics and Molecular Carcinogenesis, The Virginia Harris Cockrell Cancer Research Center at The University of Texas MD Anderson Cancer Center, Smithville, TX; ²North Houston Early College High School, Houston, TX; ³Howard University, Washington, DC; ⁴University of Houston-Downtown, Houston, TX; ⁵MD Anderson Cancer Center UTHealth Graduate School of Biomedical Sciences, Houston, TX

Triple-negative breast cancers (TNBCs), representing a broad subclass of breast cancers lacking estrogen and progesterone receptor response and HER2 amplification, are refractory to hormone-based and molecularly targeted therapies, and greater understanding of the mechanisms that drive or contribute to TNBC subtypes is needed. One of the aggressive, highly malignant types of TNBC is carcinosarcoma, or metaplastic breast cancer (MpBC), which is composed of two tissue types: carcinoma (cancer of epithelial cells) and sarcoma (cancer of connective tissues or mesenchymal cells). Targeted treatments of TNBC in general and MpBC in particular are unmet needs. To accomplish this goal, one must understand how MpBCs are initiated and the underlying molecular mechanisms that drive progression of heterogeneous carcinosarcomas. Tripartite motif containing protein 24 (TRIM24) is an oncogenic PHD/bromo histone reader and E3 ubiquitin ligase of p53 that is frequently overexpressed in mammary epithelia of breast cancer patients and linked with poor prognosis. To determine whether TRIM24 is oncogenic in vivo, we created a mouse model with conditional overexpression (COE) of TRIM24 protein in mammary epithelia (Trim24COE). Surprisingly, TRIM24 overexpression is sufficient to drive development of murine carcinosarcomas (70% of all tumors, equivalent to human MpBC), which are

highly penetrant and lack estrogen receptor, progesterone receptor, and HER2 expression. Preliminary results showed high expression of TRIM24 in MpBC patient-derived tumor arrays and xenografts, supporting TRIM24 as a relevant oncogene in human breast cancers. These findings suggest exciting opportunities to exploit the Trim24COE mouse model as a means of understanding mechanisms of MpBC development and to create a new animal model for preclinical studies of new epigenetic-based therapeutic approaches. Preliminary characterization of carcinosarcomas derived from Trim24COE mice exhibited distinct similarity with human MpBCs tumors according to immunohistochemistry. Furthermore, we determined the transcription profile of various tumor types followed by gene ontology analysis. Few of the upregulated pathways among tumors were epithelial-to-mesenchymal transition, glycolysis, or G2/M checkpoint activation. We also performed limited protein profiling of carcinosarcomas from Trim24COE mice using reverse-phase protein array analysis and found that epithelial-to-mesenchymal transition is still among the top upregulated pathways according to gene ontology analysis. In collaboration with Dr. Nathanael Gray's laboratory, we obtained a protein degrader of TRIM24, which is a potent inhibitor of the TRIM24 bromodomain. Preliminary analysis with the degrader of TRIM24 of carcinosarcoma-derived cell lines showed TRIM24 degradation within 48 hours upon treatment and decreased cell viability. Further studies will focus on determining the role of TRIM24 in carcinosarcoma both as a histone reader and as a ubiquitin ligase. We will further develop the degrader as a tool for a therapeutic approach for both a mouse carcinosarcoma model and human MpBCs.

Bilingualism in Toddlers Born Preterm: Cognitive, Language, and Brain Development

Kelly A. Vaughn, PhD¹, Johanna Bick, PhD², Janelle Montroy, PhD¹, Susan Landry, PhD¹, Dana DeMaster, PhD¹

¹Children's Learning Institute, The University of Texas Health Sciences Center at Houston, Houston, TX; ²Department of Psychology, University of Houston, Houston, TX

In the United States, about 1 in 10 infants is born before 37 weeks of gestation (i.e., preterm) (Ferre et al., 2016). Prematurity increases the risk of atypical brain development, with cascading effects on cognitive, emotion, and language development (van Noort-van der Spek et al., 2012). Also, more than a third of school-aged children in Texas are bilingual, broadly characterized as speaking a language other than English at home (Kids Count Data Center, 2018). Learning two languages early in life also impacts cognitive, language, and brain development (Ferjan Ramirez, et al., 2016; Pons, et al., 2015). However, bilingualism is not well understood in the preterm population. The goal of this investigation was to explore developmental outcomes in bilingual and monolingual toddlers born preterm. An additional goal was to explore links between parent behavior and preterm toddler outcomes in the bilingual and monolingual context. Twenty-six preterm toddlers (mean, 25.85 weeks gestation [standard deviation, 2.40 weeks]) with term-adjusted ages of 13-28 months (mean, 16.96 months [standard deviation, 4.05 months]) participated in this study. They were categorized as bilingual (n = 11), monolingual (English only; n = 10), or other (no English; n = 5) based on the language or languages spoken at home. Parenting behavior and language use measured via dyadic parent-child interactions were coded using a validated protocol. In this task, a gift was placed on a table, and parents were told to not allow the child to open the gift for 8

minutes. Frequency of parental language to distract the child from the gift (e.g., singing, telling stories) was recorded. Each child's cognitive skills were assessed using the 3-6-9 box task, in which children look inside different boxes to find new toys, which requires remembering which boxes were already searched and choosing to search different ones. Finally, magnetic resonance images of 11 infants (6 bilingual, 5 monolingual) were acquired while they were asleep to assess their brain structures. Child language was measured via parent reports using the Brief Infant Toddler Social Emotional Assessment (Briggs-Gowan et al., 2002). The frequency of parental language distraction during the dyadic interaction was positively correlated with parental reports that the child "points to show you something far away" ($r = 0.41$) and with performance of the 3-6-9 box task ($r = 0.42$). Performance of this task was positively correlated with gray matter volume in the right superior medial frontal gyrus ($r = 0.46$), which was positively correlated with gray matter volume in the right supramarginal gyrus ($r = 0.57$). Additionally, bilingual infants experienced more language distraction during the dyadic interaction ($d = 2.06$), higher parental ratings for "points to show you something far away" ($d = 0.78$), better performance on the 3-6-9 task ($d = 0.78$), and greater gray matter volume in the right superior medial frontal gyrus ($d = 1.43$) and supramarginal gyrus ($d = 1.31$) than did monolingual infants. These results provide preliminary evidence that bilingual preterm infants differ from their monolingual peers in terms of language, cognition, and brain structure. Both bilingual children and their parents use language differently than do monolingual children through pointing and distracting. Taken together, these group differences suggest that the language environments differentiate bilingual and monolingual children during development.

Caspase-2 Regulates a Cell Cycle Checkpoint to Limit Growth of Cancer Cells

Ashley Boice, PhD¹, Melissa Parsons, PhD¹, Chloe Charendoff¹, Tej Pandita, PhD²,
Lisa Bouchier-Hayes, PhD¹

¹Department of Pediatrics, Hematology-Oncology Section, Baylor College of Medicine, Houston, TX; ²Department of Radiation Oncology, Houston Methodist Research Institute, Houston, TX

Caspase-2 is the most evolutionarily conserved of the caspase family members, which are well known for their involvement in apoptosis. Caspase-2 has also been implicated in nonapoptotic processes, including a proposed role in cell division. In several murine cancer models, caspase-2 knockouts demonstrated increased tumorigenesis and genomic instability, indicating that caspase-2 is a tumor suppressor. Additionally, decreased caspase-2 expression is linked with poor prognosis in patients with acute lymphocytic leukemia or acute myeloid leukemia, emphasizing its clinical significance. Due to its implicated involvement in cancer, investigation of the role of caspase-2 in cell-cycle regulation would contribute to a better understanding the pathogenesis of cancer. To investigate the effects of caspase-2 on cell division, we measured the rate of cell proliferation in Casp2^{+/+} and Casp2^{-/-} mouse embryonic fibroblasts. We observed that Casp2^{-/-} cells proliferated at a higher rate than did Casp2^{+/+} cells as measured according to cell number and BrdU staining. Overexpression of Bcl-XL to block caspase-2-induced apoptosis failed to phenocopy the increased proliferation of the Casp2^{-/-} cells, suggesting that the increase in proliferation was not dependent on the ability of caspase-2 to induce apoptosis. We next investigated the activation of caspase-2 during cell division by employing bimolecular fluorescence complementation (BiFC) to visualize the induced proximity of caspase-2 as an indication of the first step of activation. To accomplish this,

the nonfluorescent halves of the yellow fluorescent protein Venus were fused to the prodomain of the caspase-2 monomer. When the two monomers of caspase-2 dimerize, the two halves of Venus (VN and VC) reassociate and generate a fluorescent signal (BiFC-positive). Time-lapse confocal microscopy of cycling cells revealed a higher number of BiFC-positive dividing cells than nondividing cells, demonstrating that caspase-2 is activated around the time of cell division. Additionally, immunoblotting of Casp2^{+/+} and Casp2^{-/-} cell lysates revealed decreased phosphorylation of the S-phase checkpoint proteins ATR and ATM in Casp2^{-/-} cells following S-phase arrest. We also noted increased DNA damage in Casp2^{-/-} cells by means of the DNA damage marker phosphorylated γ H2AX. Therefore, decreased activation of ATR and ATM likely reflects aberrant DNA replication, leading to increased DNA damage. To determine how this affects recovery from cell-cycle arrest, BrdU/7-AAD staining was used following S-phase arrest to approximate the relative percentage of cells in each phase of the cell cycle. A delayed exit from S phase in Casp2^{-/-} cells was observed, further supporting that caspase-2 plays an important role in S-phase progression. Consistent with this, DNA fiber experiments demonstrated that Casp2^{-/-} cells had an increased percentage of stalled forks and new replication origins. Altogether, these results support an important role for caspase-2 in cell-cycle regulation, potentially by means of ATR/ATM activation, which results in stabilized DNA replication forks, DNA repair, and proper exit from S phase. We propose that this mechanism may underlie the tumor suppressor function of caspase-2.

Decorin-Mediated Suppression of Tumorigenesis and Skin Invasion in Inflammatory Breast Cancer via Inhibition of the E-cadherin/EGFR Axis

Xiaoding Hu, MD, PhD^{1,3}, Emily Villodre, PhD^{1,3}, Richard Larson, MD^{2,3}, Omar Rahal, PhD^{2,3}, Xiaoping Wang, PhD^{1,3}, Savitri Krishnamurthy, MD^{3,4}, Debu Tripathy, MD^{1,3}, Naoto Ueno, MD, PhD^{1,3}, Wendy Woodward, MD, PhD^{2,3}, Bisrat Debeb, DVM, PhD^{1,3}

¹Department of Breast Medical Oncology, ²Department of Radiation Oncology, ³Morgan Welch Inflammatory Breast Cancer Research Program and Clinic, ⁴Department of Pathology, The University of Texas MD Anderson Cancer Center, Houston TX

Background: Inflammatory breast cancer (IBC) is a clinically distinct and highly aggressive form of primary breast cancer. Although considered rare, IBC accounts for a significant 10% of breast cancer-related deaths due to rapid proliferation and a strong propensity to metastasize to distant organs. The underlying molecular mechanisms of aggressiveness and metastasis of IBC remain elusive. Through transcriptome profiling, we identified that the small leucine-rich proteoglycan gene family member decorin (DCN) is significantly altered in metastatic IBC sublines. The aim of this study was to investigate the function and mechanism of DCN in IBC tumorigenesis and metastasis.

Methods: Three IBC cell lines (ER-/HER2+ [MDA-IBC3 and SUM190] and ER-/HER2- [SUM149]) were used in this study. DCN gene expression in clinical samples was analyzed using publicly available data sets and the Inflammatory Breast Cancer International Consortium data set. Stable overexpression of DCN in IBC cell lines (SUM149 and MDA-IBC3) was achieved using lentiviral vectors. For in vivo studies, DCN-overexpressing cell lines were injected into the cleared mammary fat pads of

SCID/beige mice, and tumor growth was monitored via caliper measurements. Tumor skin involvement was assessed visually during primary tumor growth and tumor excision. Proteomic profiling was performed using a reverse-phase protein array. Protein-protein interaction was analyzed via reciprocal immunoprecipitation of exogenous or endogenous proteins.

Results: DCN expression was significantly lower in breast tumors than in normal breast tissue ($p < 0.0001$), in aggressive breast cancer subtypes ($p < 0.0001$), and in metastatic tumors than in primary tumors ($p < 0.0001$). Moreover, high DCN expression correlated with improved overall survival ($p < 0.0001$) and relapse-free survival ($p = 0.0003$). In vitro, DCN overexpression in IBC cell lines significantly inhibited colony formation (MDA-IBC3, $p = 0.0115$; SUM149, $p = 0.0068$), migration (SUM149, $p = 0.0165$), invasion (SUM149, $p = 0.0159$), and primary and secondary mammosphere formation (primary: MDA-IBC3, $p = 0.0209$; SUM149, $p = 0.0232$; secondary: MDA-IBC3, $p = 0.01$; SUM149, $p = 0.0031$). In vivo, DCN overexpression in MDA-IBC3 cells inhibited primary tumor growth ($p = 0.0092$) and reduced skin invasion (DCN control vs. DCN overexpression, 88.9% vs 33.3%; $p = 0.017$ [chi-square test]). Analysis of our proteomic data on DCN-overexpressing SUM149 and MDA-IBC3 cells demonstrated downregulation of epidermal growth factor receptor (EGFR) and E-cadherin protein. Mechanistically, DCN reduced E-cadherin and EGFR protein expression and EGFR phosphorylation in IBC cells. Co-immunoprecipitation demonstrated that DCN physically interacts with E-cadherin in IBC cell lines. DCN downregulates E-cadherin due to reduced protein stability rather than decreased E-cadherin mRNA expression. Additionally, E-cadherin knockdown in IBC cells decreased, but its overexpression increased activation of EGFR signaling without affecting DCN expression. Furthermore, restoring E-cadherin in DCN-overexpressing IBC cell lines rescued the inhibitory effect of DCN on the activity of EGFR signaling.

Conclusions: Our results demonstrate that DCN interacts with E-cadherin to reduce its protein level and suppress the EGFR signaling pathway and that this inhibits IBC tumorigenesis and skin invasion. Our study provides new insights into and a novel mechanism of IBC pathobiology that may be therapeutically targetable. Future studies will determine the role of DCN in IBC metastasis and the detailed mechanism of DCN-mediated suppression of tumorigenesis in IBC patients.

Directed Neuronal Differentiation in GBM by Suppression of TAZ

Alessandra Audia, PhD¹, Visweswaran Ravikumar², Kunal Rai, PhD³, Arvid Rao, PhD², Jacob Hooker, PhD⁴, Krishna Bhat, PhD¹

¹Department of Translational Molecular Pathology, The University of Texas MD Anderson Cancer Center, Houston, TX; ²Department of Computational Medicine & Bioinformatics, Michigan Medicine, University of Michigan, Ann Arbor, MI; ³Department of Genomic Medicine, The University of Texas MD Anderson Cancer Center, Houston, TX; ⁴Department of Radiology, Harvard Medical School, Boston, MA

Glioblastomas (GBMs), or grade IV gliomas, are the most recalcitrant adult brain tumors, afflicting about 18,000 Americans every year with a median survival duration of only 12-15 months. Molecular classification of GBMs has shown two major subtypes—proneural (PN) and mesenchymal (MES)—based on gene expression patterns. Patients whose tumors exhibit a PN signature, or those enriched in pure PN tumor cells according to single-cell sequencing, exhibit markedly better overall survival than do those with the MES subtype. Importantly, almost all isocitrate dehydrogenase (IDH)-mutant low-grade gliomas (grades II and III) also exhibit a PN gene enrichment pattern and better survival than in patients with GBM. Of note is that a PN-to-MES switch directly contributes to treatment resistance. Therefore, suppressing the MES phenotype and resetting the PN state may be a unique therapeutic strategy for GBM. However, the molecular players that regulate PN gene expression in GBMs are unknown. We previously identified TAZ as a master transcriptional activator of the MES phenotype. We found that TAZ is epigenetically silenced in IDH-MUT/PN gliomas. TAZ in combination with platelet-derived growth factor subunit B can drive conversion of low-grade PN tumors into high-grade MES gliomas. Our preliminary investigations demonstrated that in addition to its transactivating functions, TAZ can cause active transcriptional repression of the PN

signatures, and silencing TAZ causes gain of PN signatures and increased neuronal differentiation. TAZ overexpression in IDH-MUT/PN GBM stem cells (GSCs) caused inhibition of retinoic acid neuronal differentiation, and conversely, CRISPR/Cas9-mediated knockout of TAZ in IDH-WT/MES GSCs promoted this process as judged according to alteration of genes regulating neurogenesis as well as cellular morphology resembling neurons (dendritic branching, etc.). Our preliminary data demonstrated that gliomas of the TAZ-low subtype were enriched in genes defining the PN/neuronal lineage, whereas gliomas of the TAZ-high subtype were enriched in genes defining the astrocytic lineage. Genome-wide chromatin immunoprecipitation-sequencing data showed that overexpression of TAZ in TAZ-low cells blocks PN gene expression and activates the MES program by epigenetically resetting enhancers. TAZ may directly act as an inhibitor of gene expression, a role already shown in the literature and involving the formation of a complex with histone deacetylase (HDAC) proteins. In fact, pan inhibition of HDAC class I in IDH-WT/MES GSCs resembles, if not amplifies, the phenotype observed when inhibiting TAZ. Our in vivo analysis of mice bearing IDH-WT/MES GBMs that received intraperitoneal injections of a new HDAC class I compound demonstrated a reduction in tumor growth and significant increase in survival. Taken together, our studies uncover a role for TAZ as a barrier for terminal neuronal differentiation and that differentiation therapy with HDAC inhibitors is possible for IDH-WT gliomas.

When Will the Cancer Start? Elucidating the Correlations Between Cancer Initiation Times and Lifetime Cancer Risks

Hamid Teimouri, PhD¹, Maria Kochugaeva, PhD², Anatoly B. Kolomeisky, PhD¹

¹Department of Chemistry, Rice University, Houston, TX; ²Systems Biology Institute, Yale University, West Haven, CT

Cancer is a genetic disease that results from accumulation of unfavorable mutations. As soon as genetic and epigenetic modifications associated with these mutations become strong enough, uncontrolled tumor cell growth is initiated, eventually spreading through healthy tissues. Clarifying the dynamics of cancer initiation is thus critically important for understanding the molecular mechanisms of tumorigenesis. We developed a new theoretical method to evaluate the dynamic processes associated with cancer initiation. It is based on a discrete-state stochastic description of the formation of tumors as a fixation of unfavorable mutations in tissues. Using a first-passage analysis, the probabilities of the cancer appearing and the times before it happens, which are viewed as fixation probabilities and fixation times, respectively, are explicitly calculated. Our model predicts that the slowest cancer initiation dynamics are observed for neutral mutations, whereas they are fast for both advantageous and, surprisingly, disadvantageous mutations. The method is applied to estimating the cancer initiation times from experimentally available lifetime cancer risks for different types of cancer. A high probability of a cancer occurring does not necessarily lead to a fast time for the cancer to start. Our theoretical analysis helps clarify microscopic aspects of the cancer initiation processes.

ENBPI Ligand for Ga-68: Synthesis, Radiolabeling Optimization, and Pilot Myocardial Perfusion Imaging with ECG-Gated PET

Riccardo Muzzioli, PhD¹, Federica Pisaneschi, PhD¹, Seth Gammon, PhD¹, David Piwnica-Worms, MD, PhD¹

¹*Department of Cancer Systems Imaging, The University of Texas MD Anderson Cancer Center, Houston, TX*

Cardiovascular disease remains the leading cause of mortality worldwide, accounting for 31% of all deaths. Myocardial viability is a crucial and fundamental examination in diagnosis and prognosis in patients with cardiovascular disease and has special consideration for cancer patients preparing to receive regimens of chemotherapy and immunotherapy that may impact heart health. Specifically, myocardial perfusion imaging (MPI) is a noninvasive imaging technique for quantifying blood flow in the heart and is commonly used to define areas of reversible ischemia, characterize at-risk and infarcted tissue, and assess ventricular function. At present, single-photon emission computed tomography (SPECT) and positron emission tomography (PET) are the diagnostic tests most commonly used to detect coronary artery disease and provide information on myocardial viability. Unlike in the imaging of other organs, improving the image resolution in cardiac SPECT or PET remains challenging due to inherent cardiac contraction, respiratory movement, and body motion during image acquisition. Electrocardiogram (ECG)- and respiratory-gated data acquisition and analysis recover substantial portions of the spatial resolution loss due to cardiac and respiratory motion. In ECG-gated SPECT or PET MPI, cardiac cycles are divided into temporal bins according to the cardiac cycle. ECG-gated image data sets are formed by reconstructing an image of each mutually corresponding data bin and arranging these images in a

series. This image series represents an averaged cardiac cycle, and each image corresponds to a certain phase of the cycle itself. Technetium-99m-based monocationic radiometal complexes are the most commonly used radiotracers for myocardial SPECT (e.g., technetium sestamibi). However, a limited worldwide supply of molybdenum-99 (parental isotope of technetium-99m) has stimulated research into the development of a novel MPI agent compatible with PET imaging. A radioisotope with excellent emission properties that can be used for PET MPI is gallium-68 (^{68}Ga ; $t_{1/2}$, 68 minutes), which can be produced at high purity using germanium- $^{68}\text{Ge}/^{68}\text{Ga}$ generators. A variety of multidentate ligands that form monocationic complexes have been synthesized and studied as myocardial imaging agents. Among multidentate ligands, Schiff base ligands with N_4O_2 binding cores are well known to coordinate various transition metals. The ENB ligand 1,2-ethylenediamino-bis(1-[3-isopropoxyphenyl-2-ate] methyleneamino-2,2-dimethyl)-propane is the active hexadentate ligand that is released after imidazoline ring cleavage of a heptadentate precursor treated with mild acid and a trivalent metal. Upon complexation of Ga^{3+} , the final complex forms a pseudo-octahedral geometry, in which Ga^{3+} is surrounded by four planar nitrogen atoms and two axial oxygen atoms. The trans bond average angle in the final complex is 171.6° , whereas the cis angle centered on Ga^{3+} is 90.1° , demonstrating minimal distortion from an ideal octahedral geometry and thus strong complexation of the metal and a highly stable radiotracer. Herein we report on the synthesis, radiolabeling, and characterization of ^{68}Ga -ENB and its use as a radiotracer in PET/computed tomography and ECG-gated PET experiments in small animals as a first step toward clinical development.

Heme Activates the Inflammatory Caspases to both Positively and Negatively Regulate Inflammation

Beatriz E. Bolívar, PhD, Vanda Yazdani, Jonathan M. Flanagan, PhD, Lisa Bouchier-Hayes, PhD

Department of Pediatrics, Hematology-Oncology Section, Baylor College of Medicine, Houston, TX

Hemolysis and increased levels of extracellular heme from red blood cell destruction underlie the pathophysiology of several disease states, including bacterial sepsis, malaria, and sickle cell disease. This hemolysis has been implicated in the inflammatory activation of monocytes, macrophages, and endothelial cells and often results in uncontrolled sterile inflammation that can augment susceptibility to infections. Heme has been shown to activate both TLR4 and caspase-1, potentially providing both the priming and activating signal to promote inflammasome assembly. Our data demonstrate that heme induces interleukin (IL)-1 β release and that this is increased in macrophages from sickle cell disease patients. Furthermore, using caspase bimolecular fluorescence complementation, an imaging-based technique we developed to visualize caspase-induced proximity, we showed that heme induced caspase-1, caspase-4, and caspase-5 activation in primary human macrophages in the absence of lipopolysaccharide priming. In contrast, lipopolysaccharide priming was required to induce IL-1 β release, suggesting that heme alone is sufficient to activate the inflammatory caspases but that an additional priming signal is required to ensure IL-1 β release. Loss of caspase-1 in the THP-1 monocytic cell line completely abrogated heme-induced IL-1 β release, whereas caspase-5 deletion sensitized cells to heme-induced IL-1 β release. This suggests that caspase-5 prevents IL-1 β release, possibly by inhibiting caspase-1 activity, contrary to

the expected proinflammatory role of its homolog caspase-4. Therefore, extracellular heme appears to behave as a trigger for activation of inflammatory caspase-1, caspase-4, and caspase-5, leading to both positive and negative regulation of proinflammatory cytokine release. Together, these studies provide insight into the molecular mechanisms between inflammatory caspase activation and heme-induced inflammation that may underlie the clinical manifestations of inflammation under nonpathogenic hemolysis conditions.

Utilizing Protein Chaperone Interactions to Identify Disease

Associated Mutations that Perturb Protein Folding in Cells

Brant R. Gracia, PhD¹, Kian Behmard², Georgios Karras, PhD¹

¹*Department of Genetics, The University of Texas MD Anderson Cancer Center, Houston, TX;*

²*Department of Biology, Emory University, Atlanta, GA*

Accumulation of damaging mutations of cancer-associated genes such as *BRCA1* and *FANCG* is inherent to carcinogenesis. Identifying causal mutations in a myriad of genetic alterations is challenging because the consequences of mutations depend on epigenetic contexts. The protein folding chaperones heat-shock protein 70 (HSP70) and HSP90 represent a highly conserved and ubiquitously expressed central processing hub that preserves protein homeostasis and mediates cytoplasmic protein biogenesis. Recent work from our laboratory suggests that chaperone interactions in cells can be used as diagnostic tools to pre-emptively identify protein coding mutations that perturb protein folding. We have further tested this model by investigating the impact of breast cancer-associated missense mutations in the C-terminal domain of the tumor suppressor protein BRCA1 (BRCT). To measure chaperone interactions with BRCA1-BRCT variants, we used a quantitative, high-throughput luminescence-based approach in living cells (luminescence-based mammalian interactome mapping). Mutant proteins are tagged with a 3x-FLAG tag epitope and transiently expressed in HEK293T cells stably expressing either HSP70 or HSP90 fused to a nanoluciferase reporter. Thirty-five previously characterized BRCT structural mutations were tested as proof of concept, belonging to either benign or structure-perturbing classes. Eleven of 15 benign mutations did not substantially bind to HSP70 or HSP90, and 18 of 20 structure-perturbing mutations bound to chaperones at least 4.8-fold more so than did wild-type

BRCT. Intriguingly, three of the benign mutations with intermediate chaperone interactions compared with benign and structural mutations are known to perturb the intrinsic phosphopeptide-binding activity of BRCT, suggesting that quantitative chaperone interactions in cells can report on mutations with functional consequences. Chaperone binding accurately delineates between benign and structure-perturbing BRCT mutations (83% accuracy) and outperforms standard sequence-based approaches that predict the impact of missense mutations (JPred4, 46%; PolyPhen-2, 60%). We applied this pipeline to missense mutations of FANCG, a DNA repair factor associated with the cancer predisposition syndrome Fanconi anemia (FA). Chaperone interactions for two FA-associated mutations are enriched for HSP70 binding when compared with naturally occurring polymorphisms. Using a protein complementation assay sensitive to trimeric complex formation, we found that these FA-associated mutations of FANCG reduce formation of the FA repair core complex FANCG-FANCA-FAAP20, suggesting that chaperone interactions report on structure-function perturbations associated with disease. Future work will measure the consequences of these mutations for the cancer cell phenotype in MDA-MB-436 cells. In this approach, saturation mutagenesis will be used to generate and compete all BRCA1-BRCT variants in the presence or absence of HSP90 inhibitors. Cancer mutations that depend on HSP90 for cell growth will be selectively depleted from the population and detected using deep sequencing. This approach can establish a practical approach to specifically targeting tumors harboring HSP90-dependent mutations that will be relevant for the treatment of many cancers.

Inhibition of IRE1/XBP1 Pathway Sensitizes Triple-Negative Breast Cancer Cells to Replication Stress and Radiotherapy

Dadi Jiang, PhD^{1*}, **Liang Wang, PhD^{1*}**, Charles Wang, PhD^{1,2,*}, Kathleen A. Bridges, MS¹, Xianzhou Song, PhD¹, Ling Xia, ME¹, Zhifen Yang, PhD³, Rakesh Bam, PhD³, Albert C. Koong, MD, PhD¹

¹Department of Radiation Oncology, The University of Texas MD Anderson Cancer Center, Houston, TX; ²The Drexel University College of Medicine, Philadelphia, PA; ³Department of Radiation Oncology, Stanford University School of Medicine, Stanford, CA

*Co-first authors.

Purpose: Radiation therapy causes DNA replication stress in cancer cells, which is manifested by stalled or slowed DNA replication forks and/or DNA synthesis. Unresolved replication stress induces DNA damage and genomic instability, ultimately leading to senescence or cell death. Previous studies showed that in response to replication stress, cells use a combination of ATM/ATR-mediated processes to restore homeostasis. Although the unfolded protein response has been implicated in replication stress response, the role of IRE1/XBP1, a major signaling branch of this response, is still unknown. As described herein, we investigated the contribution of IRE1/XBP1 signaling to maintenance of cellular homeostasis during replication stress and revealed that inhibition of this pathway sensitizes triple-negative breast cancer (TNBC) cells to replication stress and radiotherapy.

Methods: To assess the role of IRE1/XBP1 in replication stress, we inhibited XBP1 expression in MDA-MB-231 and other human TNBC cell lines using short hairpin RNA and evaluated the effects on cell proliferation, cell-cycle distribution, replication fork

progression, and fork restart after stalling. To evaluate the specific contribution of IRE1/XBP1 to these effects, we reintroduced XBP1 expression in cells expressing XBP1 short hairpin RNA. To determine more precisely the dependence on IRE1/XBP1 to sustain replication homeostasis, we used an inducible XBP1 short hairpin RNA system to study the kinetics of change in these assays. To further investigate the outcome of XBP1 inhibition in TNBC cells during a therapeutic intervention that induces replication stress, we performed a comet assay to assess the accumulation of DNA damage and a clonogenic survival assay after radiation treatment.

Results: Deficiency in XBP1 expression in TNBC cells significantly decreased cell proliferation. This effect was accompanied by an increased number of stalled replication forks and decreased ability to restart fork progression after stalling. The increased number of stalled forks eventually led to accumulation of single- and double-stranded DNA breaks. Consistent with these findings, XBP1 inhibition resulted in remarkable sensitivity to radiation treatment in our clonogenic survival assays.

Conclusions: Although endoplasmic reticulum stress and replication stress induce apparently distinct cellular response machineries, significant interaction and cross-talk exist between the two sets of homeostasis pathways co-stimulated by stresses from the tumor microenvironment. TNBC cells rely on IRE1/XBP1 signaling to mitigate detrimental effects following replication stress. Our findings suggest that IRE1/XBP1 inhibition and replication stress during cancer therapy reveal a novel type of synthetic lethality that may be exploited in cancer therapy.

Loss of Excitatory Cerebellar Neurons Alters Circuit Function and Causes Severe Motor Dysfunction in Neonatal Mice

Meike E. van der Heijden, PhD^{1,2}, Amanda M. Brown^{1,2,3}, Elizabeth P. Lackey^{1,2,3}, Tao Lin, PhD^{1,2}, Roy V. Sillitoe, PhD¹⁻⁴

¹Department of Pathology, Baylor College of Medicine, Houston, TX; ²Jan and Dan Duncan Neurological Research Institute of Texas Children's Hospital, Houston, TX; ³Department of Neuroscience, ⁴Program in Development, Disease Models & Therapeutics, Baylor College of Medicine, Houston, TX

Acute trauma or neurodegeneration in the cerebellum often leads to severe motor impairment and greatly diminishes the quality of life of patients with cerebellar movement disorders such as ataxia, dystonia, and tremor. A growing number of mouse models of cerebellar dysfunction recapitulate human motor disorders, with transgenic mice displaying either one disorder or combinations of them. In genetic and developmental models, motor impairments can be observed in neonates even though the cerebellar circuit is not fully developed until several weeks after birth. Thus far, most models have focused on inhibitory Purkinje cells (PCs) because they are the single output neurons of the cerebellar cortex and modulate cerebellar nuclear cells that connect the cerebellum with other parts of the central nervous system. However, the most abundant cells in the cerebellum are excitatory neurons, and most excitatory neurons are born after birth. Fast, clonal postnatal expansion of excitatory cerebellar neurons has made difficult manipulating their developmental mechanisms and studying their role in cerebellar function. The cerebellum has three types of excitatory neurons: 1) granule cells, which represent the most numerous cell type in the mammalian brain and directly modulate PCs; 2) unipolar brush cells, which are only present in specific cerebellar domains and

contribute to vestibular functions; and 3) excitatory cerebellar nuclei cells, which form the main connection between the cerebellum and cerebrum through connections with the thalamus. Of note, these three groups of excitatory neurons are all derived from the same developmental domain and require the *Atoh1* gene for development. We selectively removed *Atoh1* from cerebellar precursor cells, which diminished the number of granule cells, unipolar brush cells, and excitatory cerebellar nuclei cells in the cerebellum. Mice lacking excitatory cerebellar neurons display obvious motor dysfunction within the second week of life, consisting of dystonia, diminished righting reflexes, and action tremors that together lead to impaired mobility in the home cage and open field. These phenotypes are more severe in mice than a lack of neuronal signaling from excitatory cerebellar neurons, suggesting that excitatory neurons are essential for cerebellar development beyond providing electrical signals. Indeed, we found that loss of excitatory neurons also affects the anatomy of the cerebellum: the characteristic layered and foliated structure of the cerebellar cortex is absent, with PCs ectopically positioned anteriorly outside the cerebellum. Immunofluorescent staining showed that PCs still receive excitatory inputs from other brain regions, but the location of these synapses on the PCs is changed. Synaptic anatomical changes are supported by *in vivo* electrophysiological recordings showing that PCs do fire action potentials but that the pattern of these potentials is significantly altered. Taken together, excitatory cerebellar neurons are essential for shaping the structure and function of the neonatal cerebellum and are required for PC development even though most excitatory neurons are born after PCs. These data add to the growing body of evidence that normal cerebellar function during the early neonatal period is essential for establishing fundamental movements that are critical for early neonatal survival.

LRP1 Is a Novel Receptor that Regulates T-Cell Proliferation

Olga Sizova, PhD, Tian-Hui Yang, PhD, Qing Ma, PhD, Dan Li, PhD, Lisa S. St. John, PhD, Gheath Alatrash, DO, PhD, Jeffrey J. Molldrem, MD

Department of Hematopoietic Biology and Malignancy, The University of Texas MD Anderson Cancer Center, Houston, TX

Background: Tumor microenvironments are often immunosuppressive, and tumor-associated neutrophils play both antitumorigenic and protumorigenic roles in cancer progression. Neutrophil protumorigenic functions include promoting cancer cell proliferation and metastasis, modulation of the tumor microenvironment, and induction of immunosuppression. According to current knowledge, tumor-associated neutrophils can mediate tumor immunosuppression via secretion of 1) nitric oxide, 2) arginase-1, and 3) reactive oxygen species¹. However, evidence that neutrophils can directly inhibit antitumor immune response, specifically in tumor-associated T cells, is lacking. We have shown that membrane-bound proteinase 3 (mP3) on neutrophils and acute myeloid leukemia (AML) blasts inhibits T-cell proliferation *ex vivo* by binding to LRP1 on activated T cells². However, *in vivo* evidence of such signal transduction pathways is lacking and must be revealed. Also, how the LRP1/mP3 axis results in inhibition of T-cell proliferation is still unclear. We hypothesize that mP3 on granulocytes or AML blasts results in inhibition of T-cell proliferation upon binding to LRP1 on the surface of T cells.

Methods: To understand the mechanism of LRP1-mediated suppression of T cells, we sought to identify the downstream signaling pathway. We used a co-culture system of mP3+ THP1 cells, an AML cell line, and Jurkat cells, a T-cell line that expresses LRP1,

as well as primary cell co-culture of donor peripheral blood mononuclear cells and neutrophils.

Results: We are studying the in vivo effects of blocking LRP1 in tumor models of AML and solid cancers, such as breast cancer and melanoma, that we have established in our laboratory. Preliminary experiments with wild-type mice showed that mouse neutrophils also have the capacity to inhibit mouse T-cell proliferation. We demonstrated that LRP1 expression on Jurkat cells was significantly (threefold) increased upon CD3/CD28 activation. We confirmed using flow cytometry that mP3 expression on various AML cell lines, including THP1, is relevant to healthy donor neutrophils and AML blasts in cancer patients. We showed that co-incubation of Jurkat cells and THP1 AML cells at different cell ratios leads to significant reductions in Jurkat cell number and suppression of cell proliferation.

Conclusions: We validated the physiologically relevant in vitro and in vivo model systems in studying LRP1-dependent T-cell suppression by mP3+ granulocytes. Additionally, we provided extended mechanistical insight into the mP3/LRP1 signaling pathway. These preliminary data support the continued study of the roles of T cells and granulocytes in cancer.

References

1. Lindau D, et al., Immunology, 2013.
2. Yang T, et al., J Immunol, 2018.

Monitoring Membrane Protein Trafficking in Live Cells at Endogenous Expression Levels Using a Novel Structural Complementation Assay

Arfaxad Reyes-Alcaraz, PhD^{1,2}, Yoo-Na Lee, PhD¹, Seongsik Yun, PhD¹, Jong-Ik Hwang, PhD¹, Jae Young Seong, PhD¹

¹College of Medicine, Korea University, Seoul, South Korea; ²College of Pharmacy, University of Houston, Houston, TX

Internalization and intracellular trafficking of membrane proteins are pivotal to maintenance of physiological functions and drug action. However, robust, versatile quantitative approaches to studying such processes in real-time living systems at endogenous expression levels are still lacking. Herein we present two new structural complementation assays to quantitatively monitor membrane protein trafficking. These structural complementation assays are based on NanoBiT technology. The versatility and robustness of this approach are demonstrated by anchoring fragments of Nano Luciferase at the plasma membrane or in early endosomes to generate luminescent signals on ligand-promoted recruitment or sequestration of Nano Luciferase fragment-tagged proteins to or from specific cell membranous systems. These assays are scalable to high-throughput formats and enable quantitative pharmacological studies of membrane protein trafficking in real time, in living systems, and at the endogenous expression level, allowing for elucidation of biased trafficking molecular mechanisms of membrane protein complexes.

Oral Administration of Leucine Ameliorates Lipopolysaccharide-Induced Depression-Like Behavior

Yongfu Tang, PhD, Raafay Rishi, Elisabeth G. Vichaya, PhD, Angela M. Casaril, Bianca Ford, Robert Dantzer DVM, PhD

Department of Symptom Research, Laboratory of Neuroimmunology, The University of Texas MD Anderson Cancer Center, Houston, TX

Corresponding author: Robert Dantzer, DVM, PhD, Department of Symptom Research, Unit 1055, The University of Texas MD Anderson Cancer Center, 1515 Holcombe Boulevard, Houston, TX, 77030. E-mail: rdantzer@mdanderson.org.

Background: We have demonstrated that intraperitoneal injection of leucine abrogates lipopolysaccharide (LPS)-induced depression-like behavior in mice by blocking the L-type amino acid transporter 1 (LAT1)-dependent transport of kynurenine (KYN) into the brain. The objective of the present project is to determine whether this effect is shared by other amino acids, including an amino acid transported by LAT1 (phenylalanine) and an amino acid not transported by LAT1 (lysine).

Methods: Male CD1 mice (10-16 weeks old) were housed individually with a 12/12-hour modified dark-light cycle. Mice were handled for 1 week and habituated to intraperitoneal injection and oral gavage every day for 3 days before testing. LPS (*Escherichia coli* serotype 0127:B8; Sigma, St Louis, MO) was administered intraperitoneally at a dose of 0.83 mg/kg followed immediately by oral administration of each amino acid at a dose of 0.76 mmol/kg. Amino acids were readministered at the same dose 6 hours later. One experiment in two or three replicates was run for comparing leucine with phenylalanine, and another independent experiment in two or three replicates was run for comparing

leucine with lysine. Each experiment was organized according to a 2 (LPS vs. saline) x 3 (water, leucine [L6914; Sigma], phenylalanine [P2126; Sigma], or lysine [L5501; Sigma]) factorial design with eight or nine mice per group. The alleviating effect of leucine on LPS-induced depression-like behavior was measured according to the duration of sniffing of female urine (female urine sniffing test [FUST], 5 minutes) and duration of immobility in the forced swim test (FST). Blood and brain samples were collected for measurement of KYN and tryptophan (TRP) levels at the end of the experiment.

Results: LPS significantly reduced FUST activity and FUST sniffing and increased FST immobility. Conversely, treatment with leucine and phenylalanine reversed the effects of LPS on FUST sniffing and FST immobility. LPS significantly increased plasma and brain KYN levels and KYN/TRP ratios. These effects were attenuated by leucine and phenylalanine in the brain. LPS, leucine, and phenylalanine had no effect on brain or plasma TRP. Leucine and lysine reversed LPS-induced depression-like behavior measured according to decreased duration of sniffing female urine and increased duration of immobility in the FST. Both leucine and lysine reversed the increase in the brain KYN/TRP ratio induced by LPS but had no effect on peripheral markers of TRP metabolism. LPS, leucine, and lysine had no effect on brain or plasma TRP.

Conclusions: Oral administration of leucine and other amino acids reverses LPS-induced depression-like behavior in mice independently of their ability to compete with LAT1-dependent KYN transport into the brain. In ongoing studies, researchers are investigating the mechanisms that mediate these effects.

Acknowledgements: This work was supported by Ajinomoto Co., Inc. (Tokyo, Japan) and the NIH/NCI under award number P30CA016672.

PRINCESS: Framework for Comprehensive Detection and Phasing of SNPs and SVs

Medhat Mahmoud, PhD, Fritz Sedlazeck, PhD

Human Genome Sequencing Center, Department of Molecular and Human Genetics, Baylor College of Medicine, Houston TX

Short Illumina sequencing is the state of the art for genetics despite the fact that it misses 193 medically relevant genes and other genomic regions (e.g., STR, ALU), which have been associated with diseases. In addition, it cannot provide sufficient phasing information, which is crucial for diseases such as TPMT mutations to assess drug metabolism in a patient. Recently, long-read sequencing technologies such as those from PacBio and Oxford Nanopore Technologies have shown the ability to enhance the detection of genomic variations, including single-nucleotide variants (SNVs), structural variants (SVs), and methylation changes. Nevertheless, none of the studies thus far have detected all genomic variations, instead focusing on SNVs, SVs, or methylation changes. Furthermore, only a few studies have included phasing information to further ease the prediction of these variations onto genes and thus phenotypes. Current clinical and research studies therefore lack a comprehensive view of genomic variations, although this information is present in their sequenced data sets. Herein we introduce PRINCESS, a method that provides haplotype-resolved SNVs, SVs, and methylation changes based on a single long-read sequencing run from PacBio or Oxford Nanopore Technologies. PRINCESS automatically adapts itself to different coverage levels to optimally leverage the data set at hand. Thus, it provides comprehensive cost- and time-efficient insight into haplotype-resolved genomic variations. This information can be leveraged to simultaneously study the interaction of SNVs, SVs, and methylation changes

and their impact on phenotypic changes. PRINCESS was evaluated based on Genome in a Bottle Oxford Nanopore Technologies standards and ultralong reads as well as PacBio Continuous Long Reads (CLRs) and Circular Consensus Sequencing data. For 1 SMRT Cell CLR data, PRINCESS achieved 95% precision and 80% sensitivity for SNVs and 93% precision and 77% sensitivity for SVs on CLRs, reaching 6.9-Mb N50 phasing of SNVs and SVs. For 1 SMRT Cell Circular Consensus Sequencing data, it achieved 95% precision and 90% sensitivity for SNVs and 94% precision and 79% sensitivity for SVs, reaching an N50 of 225 kb. PRINCESS applied to 18 PacBio with matching RNA sequencing data samples improved the detection of SVs (average, 22,105), SNVs, and phasing (average, ~5 Mb N50) and thus allowed for the detection of expression quantitative trait loci in an automated, fast, comprehensive fashion.

Putting the Brakes on Translation – A Computational Study to Understand the Mechanism of Translation Inhibition by Pateamine A and Analogs

Rajan R. Chaudhari, PhD¹, Rong Chen, PhD¹, Mingzhao Zhu, PhD², Kenneth G. Hull, PhD², Daniel Romo, PhD², William Plunkett, PhD¹, Shuxing Zhang, PhD¹

¹Department of Experimental Therapeutics, The University of Texas MD Anderson Cancer Center, Houston, TX; ²Department of Chemistry & Biochemistry and CPRIT Synthesis and Drug-Lead Discovery Laboratory, Baylor University, Waco, TX

Dysregulated mRNA translation due to altered translation factors, regulators, or other components of the translation machinery is often associated with cancer proliferation, survival, invasion, angiogenesis, and metastasis. Therefore, the translation machinery is an effective target for cancer therapy. eIF4A initiation factors play an important role in translation initiation in eukaryotes. Pateamine A (PatA) is a marine natural product that inhibits cap-dependent eukaryotic translation initiation and has potent antiproliferative and proapoptotic activity. DMDAPatA (a simplified derivative of PatA) binds to plasma proteins, which limits its potency. To overcome this, a new series of PatA analogs were synthesized, and three new leads were identified with potent translation inhibitory activity. Additionally, homology models of human eIF4A1 in closed conformation were developed to understand the structural insights. PatA analogs were then docked to the predicted binding pocket, and the interactions between PatA derivatives and eIF4A1 were studied. Our computational study results suggest that PatA and its derivatives bind to a pocket located between RNA- and ATP-binding pockets. PatA analogs were found to interact with eIF4A1 residues that directly or indirectly form nonbonded interactions with RNA and ATP molecules. Additionally, these compounds interact with residues at

the C-terminal and N-terminal domains, suggesting that they stabilize the closed conformation of the eIF4A receptor, which has never been proposed before. Results from this study will be used to develop the next generation of translation inhibitors and provide hypotheses to develop experiments for studying the mechanism of action of PatA derivatives.

Mutation Status of RAS, TP53, and SMAD4 Is Superior to Mutation Status of RAS Alone for Predicting Prognosis after Resection of Colorectal Liver Metastases

Yoshikuni Kawaguchi, MD, PhD¹, Timothy E. Newhook, MD¹, Yun Shin Chun, MD, FACS¹, Ching-Wei D. Tzeng, MD, FACS¹, Thomas A. Aloia, MD, FACS¹, Scott Kopetz, MD PhD, FACP², Jean-Nicolas Vauthey, MD, FACS¹

¹Department of Surgical Oncology, ²Department of Gastrointestinal Medical Oncology, The University of Texas MD Anderson Cancer Center, Houston, TX

Introduction: Understanding of tumor biology and risk stratification based on clinicopathologic prognostic factors has improved the selection of patients for resection of colorectal liver metastases (CLMs). Recently, gene mutation analysis has been studied for its utility in identifying patients who may benefit from CLM resection. However, which combination of gene mutations implicated in prognosis after CLM resection most precisely predicts prognosis after this surgery remains to be elucidated. We aimed to determine the impact of combinations of high-frequency somatic mutations and clinicopathologic factors on survival among patients undergoing liver resection for CLMs.

Methods: We identified patients who underwent initial liver resection of CLMs during 2007-2017 and had multiple gene mutation data available. Risk factors and hazard ratios (HRs) for overall survival (OS) and recurrence-free survival (RFS) were determined using Cox proportional hazards models.

Results: Of 1,462 patients who underwent CLM resection during the study period, 507 met inclusion criteria. Multigene testing revealed that mutation rates were higher than 10% for TP53 (70.8%), APC (53.5%), RAS (50.7%), PIK3CA (15.8%), and SMAD4 (11.0%). BRAF was mutated in 2% of patients. Mutations of BRAF, RAS, TP53, and SMAD4 were significantly associated with poor OS together with clinicopathologic factors (largest CLM diameter and surgical margin status), and mutations of RAS, TP53, and SMAD4 were significantly associated with poor RFS together with demographic and clinicopathologic factors (age, number of CLMs, largest CLM diameter, prehepatectomy chemotherapy >3 months, extrahepatic disease, and surgical margin status). Patients with triple mutations of RAS, TP53, and SMAD4 had a significantly worse median OS duration (2.3 years) than did patients with double mutations (KRAS, TP53, or SMAD4; 4.5 years [HR, 3.21]; $p < 0.001$), those with single mutations (6.9 years [HR, 6.0]; $p < 0.001$), and wild-type patients (7.8 years [HR, 8.61]; $p < 0.001$). In turn, double mutations conferred significantly worse OS than did single mutations (HR, 1.88; $p < 0.001$) and wild-type status (HR, 2.68; $p = 0.002$). Patients with RAS mutations and wild-type for TP53/SMAD4 had OS and RFS durations that were not significantly different from those in patients wild-type for RAS (HR, 0.95; $p = 0.858$ and HR, 1.06; $p = 0.729$, respectively).

Discussion: Double or triple mutations of RAS, TP53, and/or SMAD4 are associated with worse survival and recurrence than are mutations of only one or none of these genes after resection of CLMs. RAS mutation status alone is not sufficient for precisely predicting prognosis. These findings may be useful for clinical decision-making for patients with tumor characteristics associated with poor prognosis and for risk stratification of patients in future clinical studies.

Role of CX3CR1 Signaling in Malignant Transformation of Gliomas

Sungho Lee, MD, PhD, Khatri Latha, PhD, Ganesh Rao, MD

Department of Neurosurgery, The University of Texas MD Anderson Cancer Center, Houston, TX

High-grade gliomas (HGGs), including the most common primary brain tumor, glioblastoma, may arise from malignant transformation of low-grade gliomas (LGGs). Whereas LGGs are often clinically indolent, glioblastomas have dismal outcomes despite maximal therapy. Accumulating data suggest that chemokine signaling directly contributes to malignant progression of LGGs by altering tumor behavior or impacting the immune microenvironment. As described herein, we examined the role of CX3CR1 signaling in malignant transformation of LGGs. First, patients with malignantly transformed LGGs were genotyped for the presence of the common loss-of-function CX3CR1 V249I polymorphism, and median overall survival was compared according to genotype. Second, RNA sequencing data were analyzed for differential gene expression based on genotype. Third, surgical samples were examined for altered expression of M2 macrophage markers and microvessel density among the genotypes. Fourth, a genetically engineered murine model was leveraged to model endogenous intracranial gliomas with targeted expression of CX3CL1 and CX3CR1 individually or in combination. Our data demonstrated that heterozygosity (V/I) and homozygosity (I/I) for the loss-of-function CX3CR1 polymorphism are associated with markedly better median overall survival in patients with LGGs that have transformed to HGGs than in those with the wild-type genotype (V/V). In addition, HGGs from patients with the V/I or I/I genotype exhibited significantly decreased levels of CCL2, which is important for the recruitment of M2 macrophages, as well as decreased levels of ANGPT1 and MMP9, which mediate

angiogenesis. This correlates with reduced intratumoral accumulation of CD204-positive macrophages and microvessel density in tumors from V/I and I/I patients. Finally, in an RCAS-PDGFB–driven model of LGG, co-expression of CX3CL1 and CX3CR1 promoted a more malignant tumor phenotype and shorter tumor-free survival. Taken together, our results demonstrate that CX3CR1 signaling promotes malignant transformation of LGGs via accumulation of glioma-associated M2 macrophages and increased angiogenesis.

Secondary Particle Interactions in a Compton Camera Designed for In Vivo Range Verification of Proton Therapy

Rajesh Panthi, PhD¹, Paul Maggi, PhD², Stephen Peterson, PhD³, Dennis Mackin, PhD¹, Jerimy Polf, PhD², Sam Beddar, PhD¹

¹Department of Radiation Physics, The University of Texas MD Anderson Cancer Center, Houston, TX; ²Department of Radiation Oncology, University of Maryland School of Medicine, Baltimore, MD; ³Department of Physics, University of Cape Town, Rondebosch, South Africa

The purpose of this study was to determine the types, proportions, and energies of the secondary radiation interactions in a Compton camera (CC) during the delivery of a clinical proton beam. The delivery of a 150-MeV clinical proton pencil beam incident on a water phantom was simulated using Geant4 software. The simulation included a CC matching the configuration of a Polaris J CC designed to image prompt gammas (PGs) emitted during proton beam irradiation for the purpose of in vivo range verification. The interaction positions and energies of the secondary radiation (gamma rays, x-rays, electrons, positrons, neutrons, and protons) were scored. The total number of secondary particles that reached the CC was found to be 157,826 counts per 10^8 protons (~ 1 Gy of dose to water). The most abundant particles were gamma rays (49.0%), neutrons (41.0%), and electrons (8.7%). The gamma rays included six major types: PGs that did not scatter before reaching the CC detector modules, PGs that were scattered in the target and/or CC box before reaching the detector modules, PGs produced from neutron-inelastic interactions, annihilation gammas, gammas produced by the neutron capture process, and radioactive-decay gammas. Only 79% of the radiation that reached the camera was found to interact in the detector modules. The amount of secondary radiation of each particle type received by each of the CC detector modules was found

to change as a function of the module's position with respect to the beam and/or the position of the Bragg peak in the target. The detector modules located in the first stage, proximal to the target, absorbed the majority of the charged secondary radiation and low-energy photons. The particle abundance of secondary neutrons and prompt gammas in two detector stages was almost constant. The count rates were lowest in the distal modules and maximal in the modules closest to the Bragg peak, ranging from 6,629 to 13,747 counts per 10^8 protons. Strategies for using CCs for proton range verification should include methods of reducing the large neutron backgrounds and low-energy non-PG radiation. The proportions of interaction types by module may provide information useful for background suppression.

Somatic ATG5 Mutations Inactivate Autophagy in Advanced Prostate Cancers by Altering a Conjugation Switch that Controls ATG12–ATG5-ATG16L1 Complex Formation

Daric J. Wible, PhD¹, Hsueh-Ping Chao, PhD¹, Tammy M. Calhoun-Davis, BS¹, Dean G. Tang, PhD², Shawn B. Bratton, PhD¹

¹Department of Epigenetics and Molecular Carcinogenesis, The Virginia Harris Cockrell Cancer Research Center at The University of Texas MD Anderson Cancer Center Science Park, Smithville, TX; ²Department of Pharmacology and Therapeutics, Roswell Park Cancer Institute, Buffalo, NY

Murine tumor models suggest that autophagy maintains homeostasis by delivering a variety of potentially oncogenic intracellular substrates to lysosomes for degradation, including excess and aberrant organelles, protein aggregates, and invading pathogens. Conversely, autophagy is reportedly activated as a survival mechanism in tumor cells in response to nutrient, oxidative, chemotherapeutic, and other stresses commonly found in the tumor microenvironment. Together, this suggests that autophagy paradoxically suppresses malignant transformation of normal cells while promoting progression and metastasis of tumor cells. Thus, inhibition of autophagy in tumor cells has intriguing therapeutic potential. However, the mechanisms by which autophagy is regulated during human tumorigenesis and the effects it has on tumor progression and metastasis are poorly understood. Of note, the 6q21 chromosomal locus containing the essential autophagy gene, autophagy-related 5 (ATG5), is among the most frequently deleted regions in human prostate cancer (PCa), and we have determined that ATG5 mRNA expression is markedly lower in both primary prostate tumors and metastases than in normal prostate tissue. The reintroduction of ATG5 into deficient prostate tumor cells

dramatically suppressed xenograft tumor growth, which, in contrast with murine tumor models, suggests that autophagy suppresses both the initiation and progression of PCa. In cells, ATG5 binds to ATG16L1 and is covalently conjugated to the ubiquitin-like protein, ATG12, to form the heteromeric ATG12–ATG5-ATG16L1 complex, which mediates autophagosome formation. We discovered that numerous somatic ATG5 mutations identified in both primary prostate tumors and metastases as well as upregulation of dominant-negative ATG16L2 expression inactivate autophagy by directly disrupting the essential ATG5-ATG16L1 interaction, which prevents ATG12 conjugation and instead triggers ubiquitin conjugation and proteasomal degradation of ATG5, ATG12, and ATG16L1. Thus, we discovered that ATG12–ATG5-ATG16L1 complex formation and autophagy are tightly regulated by a conjugation switch formed by the competing ATG12 and ubiquitin conjugation reactions that target ATG5. We determined that this conjugation switch mechanism is directly altered through multiple unique mechanisms in both primary prostate tumors and metastases, which suggests that use of autophagy inhibitors is likely contraindicated in the treatment of PCa.

Supported by the NIH (CA129521 and GM096101), the NIEHS (T32ESO7247), and MD Anderson (Institutional Research Grant).

The G-Quadruplex DNA Stabilizing Drug Pyridostatin Promotes DNA Damage and Downregulates Transcription of Brca1 in Neurons

Jose Moruno-Manchon, PhD¹, Edward Koellhoffer, PhD², Shashank Hambarde, PhD³, Nayun Kim, PhD³, Louise D. McCullough, MD, PhD², Andrey Tsvetkov, PhD^{1,4}

¹Department of Neurobiology and Anatomy, ²Department of Neurology, ³Department of Microbiology and Molecular Genetics, McGovern Medical School at The University of Texas Health Science Center at Houston, Houston, TX; ⁴MD Anderson Cancer Center UTHealth Graduate School of Biomedical Sciences, Houston, TX

The G-quadruplex is a noncanonical DNA secondary structure formed by four DNA strands containing multiple runs of guanines. The G-quadruplexes play an important role in DNA recombination, replication, telomere maintenance, and transcription regulation. Small molecules that stabilize the G-quadruplexes alter gene expression in cancer cells. We hypothesized that the G-quadruplexes regulate transcription in neurons. We discovered that pyridostatin, a small molecule that specifically stabilizes G-quadruplex DNA complexes, induced neurotoxicity and promoted the formation of DNA double-strand breaks in cultured neurons. We also found that pyridostatin downregulated transcription of the Brca1 gene, which is critical for double-strand break repair. Importantly, in an in vitro gel shift assay, we discovered that an antibody specific to the G-quadruplex structure binds to a synthetic oligonucleotide, which corresponds to the first putative G-quadruplex in the Brca1 gene promoter. Together, our results suggest that the G-quadruplex complexes regulate transcription in neurons. Studying the G-quadruplexes could represent a new avenue for neurodegeneration and brain aging research.

The Hook Complex-Associated Protein BOH1 in *Trypanosoma brucei* Cooperates with Polo-Like Kinase to Regulate Flagellum Inheritance and Cytokinesis Initiation

Kieu T.M. Pham, PhD, Qing Zhou, PhD, Yasuhiro Kurasawa, PhD, Ziyin Li, PhD

Department of Microbiology and Molecular Genetics, McGovern Medical School at The University of Texas Health Science Center at Houston, Houston, TX

The parasitic protozoan *Trypanosoma brucei* possesses a motile flagellum that also determines cell morphology, defines the cell division plane, and mediates cell-cell communications. Inheritance of the newly assembled flagellum during the cell cycle is controlled by the polo-like kinase homolog TbPLK, which also regulates cytokinesis initiation. TbPLK localizes to multiple cytoskeletal structures such as the basal body, bilobe, and distal tip of the newly assembled flagellum attachment zone (FAZ) filament. TbPLK functions upstream of the signaling pathway and recruits numerous downstream cytokinesis regulators. Mechanistically, how TbPLK is targeted to its subcellular locations to execute its multiple functions remains poorly understood. Herein we report on a novel trypanosome-specific protein named BOH1 that interacts and cooperates with TbPLK to regulate flagellum inheritance and cytokinesis initiation. BOH1 localizes to an unusual subdomain in the bilobe structure, bridging the hook complex, centrin arm, and FAZ filament. Depletion of BOH1 disrupts the hook complex morphology, inhibits centrin arm elongation, and abolishes assembly of the FAZ, leading to flagellum detachment and mispositioning. Furthermore, BOH1 deficiency impairs localization of TbPLK and the cytokinesis regulator CIF1 to the new FAZ tip, providing the molecular mechanism for its role in cytokinesis initiation. These results demonstrate the requirement of BOH1 for

maintaining bilobe morphology and regulating flagellum inheritance and identify BOH1 as an upstream regulator of the TbPLK-mediated cytokinesis regulatory pathway.

Analyzing Left-Truncated and Right-Censored HIV Cohort Data with Interval-Censored HIV Infection Onset

Daewoo Pak, PhD¹, Jun Liu, PhD², Jing Ning, PhD¹, Guadalupe Gómez, PhD³, Yu Shen, PhD¹

¹Department of Biostatistics, ²Department of Plastic Surgery, The University of Texas MD Anderson Cancer Center, Houston, TX; ³Departament d'Estadística i Investigació Operativa, Universitat Politècnica de Catalunya, Barcelona, Spain and BGSMath: Barcelona Graduate School of Mathematics

In a cohort study of HIV-infected individuals followed for the onset of AIDS, the period from HIV infection to the onset of AIDS, referred to as the incubation period for AIDS, is of main interest. However, it is often difficult to ascertain due to HIV infection onset timing/date uncertainty. An additional complication is that the observed HIV-infected subjects are likely to have long incubation periods for AIDS. We demonstrated how to estimate distribution of the incubation period of AIDS with the uncertain HIV infection onset subject to left-truncation and right-censoring. Estimation of the underlying incubation period from the HIV/AIDS cohort data is handled within a general, flexible, parametric modeling framework. The generalized odds-rate class of regression models, which consists of widely used models, proportional hazards, and proportional odds models, is considered in assessing the association of risk factors with the incubation period for AIDS. In simulation studies, we assessed the finite sample performance of the model fitting and hazard function estimation. We applied the proposed method to data from an HIV/AIDS study on intravenous drug users admitted to a detoxification program in Badalona, Spain.

Bayesian Variable Selection in Regression with Compositional Covariates

Liangliang Zhang, PhD¹, Yushu Shi, PhD¹, Kim-Anh Do, PhD¹, Robert Jenq, MD²,
Christine Peterson, PhD¹

¹Department of Biostatistics, ²Department of Genomic Medicine, The University of Texas MD
Anderson Cancer Center, Houston, TX

In clinical science, researchers often aim at identifying the bacterial taxa associated with a continuous outcome. However, these bacterial taxa are dependent on each other in a phylogenetic tree that is generated based on DNA sequence similarities. These dependences bring difficulties to regular variable selection techniques. We tackled this problem using a Bayesian variable selection framework by considering the phylogenetic tree as a graphical prior and formulated an Ising prior on the model space to incorporate structural information on candidate variables. Additionally, microbiome compositions are often defined as sparse vectors of proportions with unit sums, which are difficult to handle statistically because of both the large number of coordinates equal to zero and constraint on the sum of coordinates. We proposed two methods to relax the constraint by transforming the parameter space: contrast transformation and generalized penalization. We showed that our methods outperformed Weilin's LASSO method in different simulation scenarios. An application with COMBO 98 data showed the usefulness of our proposed model when linking the microbiome with BMI.

Enabling Communication Between Microbe-Microelectronic Interface with Incorporated Protein Switches

Taniya M. S. K. Pathiranage, PhD¹, Ian Campbell², Jonathan Silberg, PhD^{2,3}, Rafael Verduzco, PhD¹

¹Department of Chemical and Biomolecular Engineering, ²Department of Biochemistry and Cell Biology, ³Department of Systems, Synthetic, and Physical Biology, Rice University, Houston, TX

Microelectronic devices with integrated engineered proteins/microbes take advantage of the tools of synthetic biology and microelectronics to combine the sensitivity of genetic networks with the functionality of microelectronic devices. For example, synthetically engineered microbes/proteins can respond to target molecules with a measurable output and can be incorporated into not only in vitro and in vivo biosensors but also highly sensitive detectors for environmental pollutants. This study is based on both electrochemical/organic electrochemical transistor-based screening with encapsulated protein switches/engineered microbes. The electrochemical measurements of metalloproteins incorporated in these devices have demonstrated a 20-fold increase in the current response over those in previous reports. In addition, high reproducibility of redox behavior of the proteins in multiple cycles indicates the effective binding of proteins to the electrode contacts and stability proteins in the newly optimized Nafion-based electrolytes that host the proteins. The ability to activate the protein switches to generate an electrical response and changes in redox behavior with the introduction of molecules that must be screened is the basic principle behind this approach. The proposed sensors are in the process of being improved on a scale of sensitivity and device architecture to form an array of sensors for simultaneous detection of multiple

target molecules. Future goals of this project include creating portable/wearable electronics for on-site monitoring in environmental studies and medical devices.

Novel Derivatives of Anaplastic Lymphoma Kinase Inhibitors: Synthesis, Radiolabeling, and Preliminary Biological Studies of Fluoroethyl Analogues of Crizotinib, Alectinib, and Ceritinib

Bhasker Radaram, PhD, Federica Pisaneschi, PhD, Yi Rao, BS, Ping Yang, MD, David Piwnica-Worms, MD, PhD*, Mian M. Alauddin, PhD*

Department of Cancer Systems Imaging, The University of Texas MD Anderson Cancer Center, Houston, TX

*Corresponding author.

Objectives: Anaplastic lymphoma kinase (ALK), an oncogenic receptor tyrosine kinase, has emerged as a therapeutic target in various cancers, especially non-small cell lung cancer. Although several ALK inhibitors have gained regulatory approval, clinical evidence indicates that their long-term benefit is often limited by the acquisition of resistance derived from secondary point mutations in the target. Importantly, some members of this class of compounds are unable to cross the blood-brain barrier, preventing efficacy against brain metastases. Herein we report on the fluoroethyl analogs of crizotinib, alectinib, and ceritinib as potential drug candidates with improved brain penetration.

Methods: The three analogs were synthesized using fluoroethyl tosylate coupled with crizotinib, alectinib, and ceritinib, respectively. In cellulo cytotoxicity screening was performed with H2228 ALK-positive lung cancer cells and H441 ALK-negative lung cancer cells. The F-18 fluoroethyl analogs of crizotinib (^{18}F -FECrizotinib) and ceritinib (^{18}F -FECeritinib) were synthesized using [^{18}F]fluoroethyl tosylate coupled with crizotinib and ceritinib, respectively. ^{18}F -FEAlectinib was synthesized from mesylate or tosylate

precursors via direct fluorination with ^{18}F -fluoride. To study the fluoroethyl ALK inhibitor pharmacokinetics in vivo, positron emission tomography was performed using the respective F-18–radiolabeled analogs in healthy nude mice.

Results: The cytotoxicity of the fluoroethyl analogs manifested in ALK-positive H2228 cells at nanomolar potency with no significant change compared with the parent compounds. We obtained the F-18 fluoroethyl analogs of ALK inhibitors with good yields, high purity, and high specific activity. Positron emission tomography in healthy mice showed significant early brain uptake (%ID/cc) for the series as a whole (^{18}F -FECrizotinib %ID/cc, 6.6 ± 2.6 ; ^{18}F -FEAlectinib %ID/cc, 8.1 ± 2.6 ; ^{18}F -FECeritinib %ID/cc, 6.6 ± 1.8 at 5 minutes after injection), suggesting penetration of the blood-brain barrier.

Conclusion: These novel fluoroethyl ALK inhibitor analogs show promise for enhanced blood-brain barrier penetration and therapeutic potential in the central nervous system.

Activity of the Novel Aurora Kinase B Inhibitor AZD2811 in Biomarker-Defined Models of Small Cell Lung Cancer

Carminia M. Della Corte, MD¹, Liz Ajpacaja¹, Robert J. Cardnell, PhD¹, Carl M. Gay, MD, PhD¹, Qi Wang, PhD², Li Shen, PhD², Kavya Ramkumar, PhD¹, C. Allison Stewart, PhD¹, You-Hong Fan¹, Carrie Adelman, PhD³, Jon Travers, PhD³, Jing Wang, PhD³, John V. Heymach, MD, PhD¹, Lauren Averett Byers, MD, MS¹.

¹Department of Thoracic/Head and Neck Medical Oncology, ²Department of Bioinformatics and Computational Biology, The University of Texas MD Anderson Cancer Center, Houston, TX;

³AstraZeneca, Cambridge UK

Background: Aurora kinases regulate mitosis and are often upregulated. Our group and others have proven that MYC-driven small cell lung cancers (SCLCs) are vulnerable to treatment with aurora kinase A inhibitors, but their use is limited by toxicity due to high aurora kinase A expression. Aurora kinase B (AURKB) levels are variable in SCLCs, making AURKB an attractive therapeutic target. A novel AURKB inhibitor, AZD2811NP (nanoparticle), is now being investigated in relapsed SCLC patients (NCT02579226). We hypothesize that molecularly defined subsets may be sensitive to treatment with AZD2811.

Methods: We tested 50 human-derived SCLC cell lines with AZD2811 in 96-hour proliferation assays. To identify translatable biomarkers of response, we correlated half-maximal inhibitory concentration (IC₅₀) values with genomic (whole exome sequencing), transcriptomic (RNA sequencing), and proteomic (reverse-phase protein array) profiling.

Results: AZD2811 was active in a subset of SCLC cells: 13 of 30 (43%) had high sensitivity (IC_{50} , <30 nM; C_{max}), and 7 of 30 (23%) had intermediate sensitivity (IC_{50} , 30-100 nM). Comparing protein expression, we found that cMYC (fold change [FC], 2.5; $p=0.015$) and vimentin (FC, 1.66; $p=0.022$) were top biomarkers of sensitivity, whereas high E-cadherin (FC, 1.94; $p=0.046$) and BCL-2 (FC, 1.86; $p=0.032$) levels were associated with resistance. Of note, among 13 highly sensitive cells, only 5 overexpressed cMYC, highlighting that activity of AURKB inhibitors is not limited to MYC-driven SCLC. Indeed, among recently described transcription factor-defined subsets of SCLC, a majority of the NEUROD1-defined subset (cMYC-enriched) was sensitive to treatment with AZD2811 (25% of ASCL1-defined and 67% of POU2F-3-defined subsets). These data suggested that the ASCL1-defined subset includes heterogeneous subgroups that require further analysis to dissect their molecular features. Mutations in EP300, a histone acetyltransferase that controls chromatin modification and transcription, also predict sensitivity.

Conclusions: Our results show encouraging single-agent activity of AZD2811 in SCLC cells in vitro and suggest a novel biomarker-driven approach for combinations. Candidate biomarkers will be tested using samples from an ongoing clinical trial. The high BCL-2 levels observed in resistant cells provide a rationale for exploring AURKB/BCL-2 inhibitor combinations.

Activity of Venetoclax-Based Therapy in TP53-Mutated Acute

Myeloid Leukemia

Mahran Shoukier, MD, Marina Konopleva, MD, PhD, Courtney Dinardo, MD, Farhad Ravandi, MD, Michael Andreeff, MD, PhD, Guillermo Garcia-Manero, MD, Elias Jabbour, MD, Naval Daver, MD, Gautam Borthakur, MD, Naveen Pemmaraju, MD, Guillermo Montalban-Bravo, MD, Christopher Benton, MD, Nicholas Short, MD, Kapil Bhalla, MD, Jorge Cortes, MD, Hagop Kantarjian, MD, Tapan Kadia, MD

Department of Leukemia, The University of Texas MD Anderson Cancer Center, Houston, TX

Background: Mutations of TP53 are associated with low response rates for standard therapy and poor outcomes in patients with acute myeloid leukemia (AML). Combination therapy with the BCL2 inhibitor venetoclax (VEN) has emerged as an effective option for AML.

Methods: Patients with TP53-mutated AML treated with VEN from 2014 to 2018 were reviewed. Mutation testing was performed using a whole-exome next-generation sequencing panel. Patient characteristics, responses to therapy, and outcomes were analyzed.

Results: We identified 69 patients with TP53-mutated AML treated with VEN: 36 (52%) in the front-line setting and 33 (48%) in the salvage (R/R) setting (Table 1). The median follow-up durations were 4.5 months (range, 0.5-48.5 months) and 8 months (range, 1.0-46.5 months) for front-line and R/R patients, respectively. The karyotype was complex in 32 (89%) and 29 (88%) patients in the front-line and R/R cohorts, respectively. In the R/R cohort, the number of median prior treatments was two (zero to eight). VEN was

given in combination with 1) hypomethylating agents (HMAs; 87%), 2) FLAG-Ida (3%), 3) low-dose ara-C (4%), or 4) CPX-351 (6%). The overall response rates (ORRs) were 47% and 24% in the front-line and R/R patients, respectively. All six patients with negative minimal residual disease had complete cytogenetic responses after taking VEN. Some remained in complete remission (CR) for a median of 3.4 months (range, 1.7-4.7 months). Two patients (both R/R) underwent allogeneic stem cell transplantation.

Conclusion: VEN-based therapy had ORRs similar to those of HMAs alone but higher CR rates in patients with TP53-mutated AML. Larger studies with longer follow-up are needed to determine the role of VEN-based therapy in this difficult subset.

Characteristics	Front-line (n=36)	R/R (n=33)	n (%) / Median (range)	n (%) / Median (range)
Age (years)	74	67	(30-86)	(22-85)
Bone marrow blasts	25	32	(6-88)	(6-86)
Secondary AML	11	4	(31%)	(12%)
Therapy-related AML	10	6	(28%)	(18%)
Karyotype				
Complex (≥ 3 abnormalities)	32	29	(88%)	(88%)
Diploid	1	1	(3%)	(3%)
Other	3	3	(9%)	(9%)
VEN combination				
VEN + HMAs	33	27	(91%)	(82%)
VEN + FLAG-Ida	0	2	(6%)	
VEN + LDAC	3	0	(6%)	(3%)
VEN + CPX-351	1	3	(3%)	(9%)

Response

CR 13 (36%) 5 (15%)

CR without count recovery (CRi) 4 (11%) 3 (9%)

ORR (CR/CRi) 17 (47%) 8 (24%)

Minimal residual disease Negative 5 (14%) 1 (3%)

Median overall survival duration (months) 3.6 2.5

6-month OS 36% 27%

Median CR duration (CRD) (months) 6.4 3.6

6-month CRD 51% 22%

Are We Appropriately Depicting Diversity: Portrayal of Skin Tone in Gender-Affirming Literature

Matthew J. Davis, BS¹, Amjed Abu-Ghname, MD¹, Nicole A. Seebacher, PhD², Jacson K. Shen, BA², Kian Adabi, BA³, Cameron J. Kneib, BS⁴, Jonathan P. Massie MD⁵, Shane D. Morrison, MD, MS⁴, Marco Maricevich, MD¹

¹Division of Plastic Surgery, Department of Surgery, Baylor College of Medicine, Houston, TX;

²Faculty of Medicine, The University of Sydney, Sydney, Australia; ³Montefiore Medical Center,

Albert Einstein College of Medicine, Bronx, NY; ⁴Division of Plastic Surgery, Department of Surgery,

University of Washington School of Medicine, Seattle, WA; ⁵Division of Plastic Surgery, Department of Surgery, Feinberg School of Medicine at Northwestern University, Chicago, IL

Background: In 2016, the percentage of nonwhite transgender individuals was estimated to be 45%, which is higher than the percentage of nonwhite individuals in the nontransgender population^{1,2}. However, ethnic representation through published images may not accurately represent the racial diversity among transgender people, as image selection can be subjective to authors' unconscious biases. Representation in the literature may thus tend toward pre-existing racial inequities and influence the accessibility, delivery, and quality of transgender health care³.

Aim: The objective of this study was to determine if published figures across the gender-affirming literature accurately reflect the racial demographics of transgender individuals.

Method and Measures: A search of all transgender health publications up to 2018 for photographs and rendered graphics depicting human skin was conducted. For each image, skin tone was categorized as light (1-2), medium (3-5), or dark (6-10) based on

the Massey-Martin scale. Proportional data and average number of dark images per article were compared. Regression analyses were performed to assess the correlation of time and geographic region on nonwhite images.

Results: In total, 2,022 photographs and 288 graphics from 291 articles were analyzed, the majority of which were of European origin (62.1%). Dark skin images represented 7.1% of photographs and 6.2% of graphic illustrations. The mean number of photographs per article with light skin was 4.9 compared with 1.5 and 0.5 with medium and dark skin, respectively ($p < 0.001$). International publications were less likely to publish photographs of dark skin than were American publications ($r = -0.317$; $p < 0.001$). Furthermore, a significant decrease in dark skin photographs over time was demonstrated ($r = -0.118$; $p = 0.046$).

Conclusions: Although the ethnic diversity of the transgender population has been well documented, racial minorities remain underrepresented across the literature, causing further marginalization of these groups. Representation of diversity in the literature is only one piece of the racial inequities in health care and should be addressed by dispelling implicit biases and cultural competencies. Moving forward, published images should better represent the true racial composition of transgender individuals.

References

1. Flores AR, Brown TN, Herman JL. Race and ethnicity of adults who identify as a transgender in the United States. UCLA: The Williams Institute. Accessed at <https://escholarship.org/uc/item/69j3q4n0>. 2016.
2. Crissman HP, Berger MB, Graham LF, et al. Transgender demographics: a household probability sample of US adults, 2014. *Am J Public Health* 2017;107(2):213-215.

3. Sabin J, Nosek BA, Greenwald A, et al. Physicians' implicit and explicit attitudes about race by MD race, ethnicity, and gender. *J Health Care Poor Underserved* 2009;20(3):896-913.

Assessment of Intratumoral Heterogeneity in Early-Stage Estrogen Receptor-Positive Breast Cancer

Sofia Mastoraki, PhD¹, Juliana Navarro-Yepes, PhD¹, Tuan Tran², Min Hu², Aysegul Sahin, MD³, Kelly Hunt, MD, FACS⁴, Nicholas Navin, PhD², Khandan Keyomarsi, PhD¹

¹Department of Experimental Radiation Oncology, ²Department of Genetics, ³Department of Pathology, ⁴Department of Breast Surgical Oncology, The University of Texas MD Anderson Cancer Center, Houston, TX

Introduction: Tumor heterogeneity is a hallmark of cancer, and its underlying clinical relevance has been well established across different tumor types. In the context of estrogen receptor (ER)-positive breast tumors, variation in ER expression among different tumors or distinct cell populations within a single tumor are predicted to account for differences in clinical behavior, treatment response, and disease recurrence. However, a clear understanding of the molecular and cellular mechanisms of tumor heterogeneity that are relevant to the prognosis and therapy for early-stage ER-positive breast cancer has not been established. Previous results of bulk RNA sequencing (RNA-seq) of ER-positive biopsy samples represent an average of gene expression patterns; this may obscure biologically relevant differences between cells. Single-cell RNA-seq (scRNA-seq) is an approach to overcoming this problem, allowing for assessment of intratumoral cell populations and biological systems at unprecedented resolution. In this study, our aim was to compare gene expression profiles for bulk RNA-seq and scRNA-seq of tumor biopsy samples in early-stage ER-positive patients.

Methods: Tumor and normal tissue biopsy samples obtained from ER-positive patients were divided into three parts: two dissociated by enzymatic disaggregation and one by

direct total RNA isolation. Tumor samples were subjected to both scRNA-seq and bulk RNA-seq analyses, whereas a single-cell suspension of normal matched tissue was used for bulk RNA-seq alone. Furthermore, patient-derived organoids were generated from both normal and tumor samples. Single-cell isolation and barcoding were assessed using the 10x Genomics technology followed by RNA-seq with the Illumina NovaSeq 6000 system (50PE), whereas bulk RNA-seq was performed using an Illumina PE150 strategy.

Results: Our preliminary data represent an assessment of tumor and adjacent normal tissue samples collected after mastectomy from an 80-year-old ER-positive, progesterone receptor-positive, HER2-negative patient diagnosed with early-stage infiltrating ductal carcinoma in situ (stage IB). ScRNA-seq of tumor tissue from this patient identified 10 distinct clusters of cells consisting of both immune and nonimmune stromal populations (epithelial cells, endothelial cells, fibroblasts, and immune cells). Ninety-five percent of single cells were luminal. However, a small group (2%) of cells had a basal-like signature, which can lead to disease recurrence. Of note, although the patient was clinically characterized as HER2-negative according to immunohistochemistry and fluorescence in situ hybridization, we observed HER2 overexpression in the vast majority (95%) of isolated single cells. Furthermore, organoid cultures recapitulated the features of patients' tumors and presented similar transcriptomic profiles. We have adapted similar sequencing and downstream analyses for an additional number of patient biopsies. Our ongoing study is geared toward comparing bulk and single cell transcriptome profiles from these ER-positive cases and identifying overlapping populations that can predict recurrence or novel therapeutic vulnerabilities.

Conclusions: Bulk RNA-seq approaches lack the resolution needed to visualize the true extent of stromal heterogeneity and may mask rare populations or cellular phenotypes that could be critical for tumor survival. ScRNA-seq highlights the dynamic and adaptive nature of all cellular populations within an evolving tumor microenvironment and reveals potential cross-talk between these two compartments. Lastly, establishment of organoid cultures presents the opportunity for high-throughput drug screening studies and the identification of new patient-tailored therapeutic strategies.

Roles of Glutamate Receptors in the Retinal Calcium Influx at Connexin 36 Gap Junctions

Yuan-Hao Lee, PhD¹, Alice Z Chuang, PhD¹, Ya-Ping Lin¹, John O'Brien, PhD^{1,2}

¹Department of Ophthalmology and Visual Science, The University of Texas Health Science

Center at Houston, Houston, TX; ²MD Anderson Cancer Center UTHealth Graduate School of Biomedical Sciences, Houston, TX

Gap junctions in the retinal inner plexiform layer play an important role in quick vision adaption to light through synaptic networks. The electrical coupled network via connexin 36 (Cx36) gap junctions is modifiable via interaction with Ca²⁺/calmodulin-dependent kinase II. Herein we describe a highly controlled multiloop circuit in which Cx36 gap junctions are in contact with calcium. In compliance with a protocol approved by the Institutional Review Board of The University of Texas Health Science Center at Houston, transgenic Cx36-GCaMP mice were used for calcium live imaging and immunostaining. Through baseline fitting, changes in GCaMP fluorescence were measured using area under the curve and analyzed using mixed linear models in RStudio. Administration of an *N*-methyl-D-aspartate (NMDA) receptor inhibitor or blocker of L-type calcium channels significantly reduced the confluence of calcium (indicated by GCaMP response) in proximity to Cx36 gap junctions upon the stimulatory input of glutamate and glycine. In contrast, GCaMP response toward α -amino-3-hydroxy-5-methyl-4-isoxazolepropionic acid (AMPA) input was significantly reduced by the inhibition of GABA_A receptors, suggesting that increasing excitatory synaptic activity leads to a decrease in synaptic AMPA receptors. Finally, the rates of co-localization of Cx36-GCaMP protein with immunostained GluR2/3 and NMDA receptor 1 were 43.6% and 62.3%, respectively. These results demonstrated the roles of glutamatergic receptors in

regulating calcium influx at Cx36 gap junctions. In conclusion, the calcium influx elicited by AMPA receptor activation correlates with the opening of GABA receptors, presumably via membrane hyperpolarization-induced AMPA receptor retention. In addition to the interplay of AMPA and GABA receptors, excitatory postsynaptic potential-induced calcium influx was dependent on the activity of NMDA receptors and L-type calcium channels. This study of calcium dynamics provides insight into how electrical synaptic transmission is regulated in the locality of Cx36 gap junctions. This project was supported by a National Eye Institute grant (R01EY012867).

IL-6 Gene Expression in Primary Acral Lentiginous Melanoma As a Clinical Prognostic Factor

Chantal Saberian, MD¹, Phyu Aung, MD, PhD², Cara Haymaker, PhD³, Salah Bentebibel, PhD¹, Daniel Johnson, MD¹, Chantale Berantchez, PhD³, Carlos Torres-Cabala, MD², Adi Diab, MD¹

¹Department of Melanoma Medical Oncology, ²Department of Pathology, ³Department of Translational Molecular Pathology, The University of Texas MD Anderson Cancer Center, Houston, TX

Background: Acral lentiginous melanoma (ALM), a rare subtype of cutaneous melanoma (CM), is of particular interest because it is more aggressive and treatment-resistant than nonacral CM.

Method: The gene expression profiles of 19 ALM and 10 nonacral CM tissue samples (formalin-fixed, paraffin-embedded) banked from 2008 to 2019 at The University of Texas MD Anderson Cancer Center were assessed using NanoString technology with a PanCancer Immune Profiling Panel.

Results: Of the patients with ALM, 15 were white, 3 were Hispanic, and 1 was Asian. Of the 10 nonacral CM patients, nine were white, and one was African American. Eighteen patients (62%) were male, and the mean patient age was 62 years (range, 2-92 years). The volar surface was the most common anatomical site of ALM (n = 17 [89%]). Of note, we found similar expression of inhibitory immune-regulatory genes in both acral and nonacral CM (CTLA4, CD274, PD-L2, FoxP3, and p53). Gene expression analysis showed that hallmark melanoma genes (MAGEA12 and PRAME) were similarly

expressed in acral and nonacral CM. Furthermore, gene expression associated with cytotoxic T cells (CD3G, CD8, IFN γ , PRF1, GZMB, and GZMA), natural killer cells (KLRD1 and KLRG1), and macrophages (CD68 and CD163) did not differ significantly in ALM and CM ($p>0.1$). In addition, we found higher expression of the IL-6 gene in primary ALM than in primary nonacral CM ($p=0.01$). Nine primary ALM patients (47%) had distant metastasis. We found high expression of IL-6 in eight primary ALM patients (42%). Seven of these eight patients (88%) had metastatic relapse, compared with two of nine patients who had low expression of the IL-6 gene ($p=0.01$).

Conclusions: In our preliminary data, we found high expression of the IL-6 gene in primary ALMs in most patients who had distant metastasis. IL-6 could be a negative clinical prognostic factor for patients with primary ALM. Additional studies with larger samples are necessary to validate these findings.

The Gender-Nonconforming Population in a Medicaid Managed Program

Amjed Abu-Ghname, MD¹, Luke Grome, MD¹, Sarth Raj¹, Marni Axelrad, MD², Stephanie Chapman, PhD²

¹Division of Plastic Surgery, Department of Surgery, ²Department of Pediatrics, Psychology Section, Baylor College of Medicine, Houston, TX

Background: With the increasing cultural awareness of gender diversity, transgender individuals are becoming more likely to present in general health care settings. In addition to traditional health care, patients in this population have unique needs related to gender transitioning. Whereas challenges related to health care utilization in this population have been discussed, studies examining health services in the Medicaid population are limited.

Aim: In this study, we addressed this knowledge gap by investigating transgender patients' use of health care services, including behavioral therapy, primary care, endocrinology, and surgery, in a Medicaid managed care program.

Methods and Measures: Following our institution's Institutional Review Board approval, a retrospective review of all patients who presented for any service billed to health insurance with gender identity disorder or gender dysphoria from 2013 to 2018 was performed. Our health plan is a Medicaid managed care organization serving almost 430,000 members in one of the largest urban areas in the United States. Information regarding patient demographics and health care services was reviewed. The utilization rates of distinct services and interventions were analyzed. No community participation

was performed. For age subanalysis, patients were placed in three groups: early adolescents (<16 years old), late adolescents (16-18 years old), and adults (>18 years old).

Results: We identified a total of 192 patients with 787 documented encounters. The mean patient age was 15.0 years (3.8-28.8 years), and the majority were early adolescents (57.8%). Assigned gender at birth was as follows: 70 male and 122 female. The mean number of encounters per patient was 4.1 (1.0-74.0). Early adolescents had the highest number of encounters followed by late adolescents and adults. Behavioral health services were the most commonly used (50.0%) followed by primary care (47.4%). Endocrinology and surgical services were encountered by 2.1% of the patients and no patients, respectively. Medications were prescribed for 25% of the population; the majority were behavioral health medications. Hormonal treatment was prescribed for 6.7% of the patients.

Conclusion: Gender identity is not a binary concept, and individuals with gender dysphoria or who identify differently from their assigned gender are an underserved population with unique health care needs. This study highlights the deficiencies in services this population is receiving under one managed Medicaid program. Whereas behavioral health services are widely employed, underutilization of medical and surgical consults compromises patient awareness of available interventions. Moving forward, we believe that a multidisciplinary clinical approach to streamlining patient care is necessary.

The Pleiotropy Associated with De Novo Variants in CHD4, CNOT3, and SETD5 Extends to Moyamoya Angiopathy

Amélie Pinard, PhD¹, Stéphanie Guey, MD, PhD², Dongchuan Guo, PhD¹, Alana C. Cecchi¹, Natasha Kharas³, Stephanie Wallace¹, Ellen Regalado¹, Ellen M. Hostetler¹, Anjail Sharrief, MD, MPH⁴, Françoise Bergametti, PhD², Manoelle Kossorotoff, MD⁵, Dominique Hervé, MD⁶, Markus Kraemer, MD⁷, Michael Bamshad, MD⁸, Deborah Nickerson, PhD⁹, Edward Smith, MD¹⁰, Elisabeth Tournier-Lasserre, MD^{2,11}, Dianna Milewicz MD, PhD¹

¹Department of Internal Medicine, ³Department of Neurobiology and Anatomy, ⁴Department of Neurology, McGovern Medical School at The University of Texas Health Science Center at Houston, Houston, TX; ²INSERM UMR-S1161, Génétique et physiopathologie des maladies cérébrovasculaires, Université Paris Diderot, Sorbonne Paris Cité, Paris, France; ⁵AP-HP, French Center for Pediatric Stroke and Pediatric Neurology Department, University Hospital Necker-Enfants Malades, Paris; ⁶AP-HP, Service de neurologie, Centre de Référence des Maladies Vasculaires Rares du Cerveau et de L'oeil, Groupe Hospitalier Lariboisière Saint Louis, Paris, France; ⁷Department of Neurology Alfried Krupp-Hospital, Essen and Department of Neurology, Medical Faculty, Heinrich-Heine-University, Düsseldorf, Germany; ⁸Division of Genetic Medicine, Department of Pediatrics, ⁹Department of Genome Sciences, University of Washington, Seattle, WA; ¹⁰Department of Neurosurgery, Boston Children's Hospital, Harvard Medical School, Boston, MA; ¹¹AP-HP, Service de génétique moléculaire neurovasculaire, Centre de Référence des Maladies Vasculaires Rares du Cerveau et de l'oeil, Groupe Hospitalier Saint-Louis Lariboisière, Paris, France

Purpose: Moyamoya angiopathy (MMA) is a very rare cerebrovascular disease characterized by bilateral stenosis or occlusion of the distal internal carotid arteries at the base of the brain with compensatory collateral vessel formation leading to strokes in

childhood and the fourth decade of life. Twelve altered genes that predispose individuals to MMA are known, but the majority of cases do not have identified genetic triggers. Therefore, we sought to identify them.

Methods: We performed whole exome sequencing of samples from 39 trios (affected children and their unaffected parents). Peddy software was used to check the quality of the sequencing data and the relationships among the samples. Gemini software was used to identify rare (minor allele frequency, $\leq 0.01\%$ in the control population in the gnomAD database) predicted pathogenic (Combined Annotation Dependent Depletion score, ≤ 20) variants following de novo transmission (present in the child, absent in the parents).

Results: We identified de novo variants of two known genes—RNF213 ($n = 3$) and NF1 ($n = 1$)—and three novel genes—CHD4 ($n = 1$), CNOT3 ($n = 2$), and SETD5 ($n = 1$). A cohort of 158 additional unrelated probands provided further proof that rare pathogenic variants of CHD4 ($n = 6$), CNOT3 ($n = 2$), and SETD5 ($n = 2$) predispose individuals to MMA. Previous studies identified de novo variants of these genes in children with developmental disorders, intellectual disability, and congenital heart disease. Phenotypic similarities between our MMA patients harboring de novo variants and those previously reported—neurodevelopmental abnormalities and head, eye, ear, nose, and throat abnormalities—expand the pleiotropy associated with de novo variants of CHD4, CNOT3, and SETD5 to include MMA.

Discussion and Conclusion: These genes encode proteins involved in chromatin remodeling and, taken together with previously reported genes leading to MMA-like cerebrovascular occlusive disease (YY1AP1 and SMARCAL1), implicate disrupted

chromatin remodeling as a molecular pathway predisposing patients to large artery occlusive cerebrovascular disease. Furthermore, these data expand the spectrum of phenotypic pleiotropy due to genetic alteration of CHD4, CNOT3, and SETD5 beyond developmental disorders to later onset disease in the cerebrovascular arteries, thus emphasizing the need to assess the clinical complications into adulthood for genes associated with developmental disorders.

The Relationship Between Alcohol, Physical Activity, and Obesity in Mexican-Origin Adults

Natalia I. Heredia, PhD¹, Qiong Dong², Shine Chang, PhD², Lorna McNeill, PhD¹

¹Department of Health Disparities Research, ²Department of Epidemiology, The University of Texas MD Anderson Cancer Center, Houston, TX

Background: Alcohol consumption, lack of physical activity (PA), and obesity are all cancer risk factors that have the potential to co-occur. Although PA and alcohol consumption have been positively associated in some racial/ethnic groups, this relationship is less studied in Hispanics. Whereas PA has had a consistent inverse relationship with obesity, the relationship between alcohol consumption and obesity is more nuanced, with current drinkers having lower risk of obesity than never-drinkers. The first aim of this study was to assess the relationship between alcohol intake and PA in Hispanic adults. The second aim was to assess the independent and interactive effects of PA and alcohol consumption on obesity and evaluate how this relationship differs according to sex and country of birth.

Methods: Data from the Mano a Mano Cohort of Mexican-origin individuals living in the greater Houston area were used. Only individuals recruited into the cohort since 2012 were included. Trained field staff measured their height and weight. Data were collected with interviewer-administered questionnaires, which included self-reported PA, alcohol intake (never-drinker, former drinker, or current drinker), and demographic characteristics. PA was categorized as high ($\geq 1,500$ MET minutes/week), moderate (≥ 600 MET minutes/week), or low (all others). Logistic regression was used to assess

the association of PA and alcohol consumption with obesity and body mass index (BMI), including an interaction term in the model.

Results: The study participants (n = 3,897) had an average age of 49 years, were mostly women, and had not attained a high school degree. Most were obese (60%) and never-drinkers (67%). More never-drinkers had low levels of PA (42%) than moderate (32%) or high (26%) levels. More current drinkers had high PA levels (32%) than did never-drinkers (26%) and former drinkers (24%). Obese individuals did less PA and had a greater proportion of never-drinkers when compared with nonobese individuals. A high PA level was protective against obesity in the entire sample (adjusted odds ratio [AOR], 0.81 [95% confidence interval (CI), 0.68-0.95]; $p < 0.05$), female subjects (AOR, 0.73 [95% CI, 0.60-0.89]; $p < 0.01$), and those born in Mexico (AOR, 0.79 [95% CI, 0.66-0.95]; $p < 0.05$). Current drinking was protective against obesity in Mexican-born individuals (AOR, 0.77 [95% CI, 0.61-0.97]; $p < 0.05$) and was associated with significantly low BMIs in the full sample, male subjects, and Mexican-born individuals. Among never-drinkers, compared with those with low PA levels, those with high PA levels were markedly less likely to be obese (AOR, 0.79 [95% CI, 0.65-0.96]). The only significant interaction between PA and alcohol use was in male never-drinkers: compared with those who had low PA levels, those with high PA levels had significantly higher BMIs (beta, 2.67 [95% CI, 1.02-4.32]).

Conclusions: In this study of Mexican-origin adults, almost half were obese and never-drinkers. Both high PA level (vs. low PA level) and current drinking status (vs. never-drinking) were independently protective against obesity. However, in the full sample and most subgroups, never-drinkers with high PA levels (vs. no PA) were the only subjects

significantly protected against obesity. These results can inform cancer prevention interventions in Mexican-origin adults.

Analyzing Astrocyte Regulation of the Blood-Brain Barrier

Nejla Yosef, PhD, Joseph McCarty, PhD

Department of Neurosurgery, The University of Texas MD Anderson Cancer Center, Houston, TX

The blood-brain barrier (BBB) partitions the circulation from the brain microenvironment. The BBB protects the brain from unwanted circulatory substances, supports the unique metabolic needs of the brain, and provides a stable environment for brain homeostasis. The BBB is also one of the most significant limitations in delivering drugs to treat brain pathologies, including neurodegeneration and cancer. Therefore, identifying key pathways that can be modulated to allow reliable, effective delivery of drugs to the brain is a critical need. The BBB is maintained through complex interactions among cells of the neurovascular unit, which comprises endothelial cells (ECs), pericytes, astrocytes, microglia, and neurons. These cell-cell interactions precisely control which factors enter and exit the brain. Growing evidence demonstrates that astrocytes play crucial roles in regulating EC barrier function¹⁻³, making them excellent candidates to study BBB modulation. Nevertheless, recent evidence demonstrates that astrocytes display functional heterogeneity that may be related to differences in their regional location in the brain^{4,5}. Perivascular astrocytes (PAs) are the most abundant astrocyte type in the neurovascular unit, where their end feet cover nearly 80% of the cerebral vascular surface and perform a wide array of functions. PAs are of particular interest in light of increased evidence that disruption of PA-vascular coupling by glioma cells is associated with increased tumor invasion⁴. Despite several studies demonstrating that PAs play important roles in maintaining the integrity of the BBB, very little is known about the molecular properties of PAs, how PAs and ECs interact to maintain proper BBB functions, or how these events are altered in cancer. This is due to a lack of suitable in vivo models that

selectively distinguish PAs from other astroglial cell populations. As an important first step in deciphering this unique biology, we generated a genetically engineered mouse model (*Mlc1-EGFP*) in which EGFP is selectively expressed in PAs⁶. Using this novel mouse model, we established an efficient protocol to fractionate *Mlc1-EGFP*⁺ cells from the cortices of adult *Mlc1-EGFP* mice using fluorescence-activated cell sorting. Further marker analysis showed that *Mlc1-EGFP*⁺ cells express *Mlc1* and other astrocyte markers. A purified PA population is suitable for a wide range of molecular and functional studies to define specialized properties that regulate BBB function and homeostasis.

References

1. Lien CF, Mohanta SK, Frontczak-Baniewicz M, et al. Absence of glial α -dystrobrevin causes abnormalities of the blood-brain barrier and progressive brain edema. *J Biol Chem* 2012;287:41374-41385.
2. Abbott NJ, Rönnbäck L, Hansson E. Astrocyte-endothelial interactions at the blood-brain barrier. *Nat Rev Neurosci* 2006;7:41-53.
3. Abbott NJ. Astrocyte-endothelial interactions and blood-brain barrier permeability. *J Anat* 2002;200:629-638.
4. John Lin CC, Yu K, Hatcher A, et al. Identification of diverse astrocyte populations and their malignant analogs. *Nat Neurosci* 2017;20:396-405.
5. Matias I, Morgado J, Gomes FCA. Astrocyte heterogeneity: impact to brain aging and disease. *Front Aging Neurosci* 2019;11:59.
6. Toutouchian JJ, McCarty JH. Selective expression of eGFP in mouse perivascular astrocytes by modification of the *Mlc1* gene using T2A-based ribosome skipping. *Genesis* 2017;55:e23071.

Novel Derivatives of Anaplastic Lymphoma Kinase Inhibitors: Synthesis, Radiolabeling and Preliminary Biological Studies of Fluoroethyl Analogues of Crizotinib, Alectinib and Ceritinib

Bhasker Radaram, PhD, Federica Pisaneschi, PhD, Yi Rao, Ping Yang, MD, David Piwnica-Worms, MD, PhD*, and Mian M. Alauddin, PhD*

Department of Cancer Systems Imaging, The University of Texas MD Anderson Cancer Center, Houston, TX

Objectives: Anaplastic lymphoma kinase (ALK), an oncogenic receptor tyrosine kinase, has emerged as a therapeutic target in various cancers, especially non-small cell lung cancer. Although several ALK inhibitors have gained regulatory approval, clinical evidence indicates that long term benefit is often limited by the acquisition of resistance deriving from secondary point mutations in the target. Importantly, some members of this class of compounds are unable to cross the blood-brain barrier, preventing efficacy in brain metastases. Herein, we report the fluoroethyl analogues of Crizotinib, Alectinib and Ceritinib as potential drug candidates with improved brain penetration.

Methods: The fluoroethyl analogues of Crizotinib, Alectinib and Ceritinib were synthesized using fluoroethyl tosylate coupled with Crizotinib, Alectinib, Ceritinib, respectively. *In cellulo* cytotoxicity screening was performed in ALK-positive lung cancer H2228 cells and ALK-negative lung cancer H441 cells. The F-18-fluoroethyl analogues of Crizotinib (^{18}F -FECrizotinib), Ceritinib (^{18}F -FECeritinib) were synthesized using [^{18}F]fluoroethyl tosylate coupled with Crizotinib, Ceritinib, respectively. [^{18}F]-FEAlectinib was synthesized from mesylate or tosylate precursors by direct fluorination with ^{18}F -fluoride. To study the fluoroethyl ALK inhibitors pharmacokinetics *in vivo*, positron

emission tomography (PET) imaging was performed using the respective F-18 radiolabeled analogues in healthy nude mice.

Results: Cytotoxicity of fluoroethyl analogues in ALK-positive H2228 cells showed up to nanomolar potency, with no significant change compared to parent compounds. The F-18-fluoroethyl analogues of ALK inhibitors were obtained with good yields, high purity and high specific activity. PET imaging in healthy mice showed significant early brain uptake (%ID/cc) for the series as a whole (^{18}F -FECrizotinib %ID/cc: 6.6 ± 2.6 ; ^{18}F -FEAlectinib %ID/cc: 8.1 ± 2.6 ; ^{18}F -FECeritinib %ID/cc: 6.6 ± 1.8 at 5 minutes post injection) suggesting penetration of the blood brain barrier.

Conclusion: These novel fluoroethyl ALK inhibitor analogues show promise for enhanced blood brain barrier penetration and therapeutic potential in the central nervous system (CNS).

This article was published in European Journal of Medicinal Chemistry, 182, Bhasker Radaram, Federica Pisaneschi, Yi Rao, Ping Yang, David Piwnica-Worms*, Mian M. Alauddin*, Novel Derivatives of Anaplastic Lymphoma Kinase Inhibitors: Synthesis, Radiolabeling and Preliminary Biological Studies of Fluoroethyl Analogues of Crizotinib, Alectinib and Ceritinib 111571, Copyright Elsevier (2019).